

The public reporting burden for this collection of information is estimated to average 1 hour per response, including the time for reviewing instructions, searching existing data sources, gathering and maintaining the data needed, and completing and reviewing the collection of information. Send comments regarding this burden estimate or any other aspect of this collection of information, including suggestions for reducing this burden, to Washington Headquarters Services, Directorate for Information Operations and Reports, 1215 Jefferson Davis Highway, Suite 1204, Arlington VA, 22202-4302. Respondents should be aware that notwithstanding any other provision of law, no person shall be subject to any penalty for failing to comply with a collection of information if it does not display a currently valid OMB control number.
PLEASE DO NOT RETURN YOUR FORM TO THE ABOVE ADDRESS.

1. REPORT DATE (DD-MM-YYYY) 28-11-2015	2. REPORT TYPE Final Report	3. DATES COVERED (From - To) 26-Sep-2014 - 25-Jun-2015
---	--------------------------------	---

4. TITLE AND SUBTITLE Final Report: Optical Force Theory	5a. CONTRACT NUMBER W911NF-14-1-0606
	5b. GRANT NUMBER
	5c. PROGRAM ELEMENT NUMBER 611102

6. AUTHORS Kevin Webb	5d. PROJECT NUMBER
	5e. TASK NUMBER
	5f. WORK UNIT NUMBER

7. PERFORMING ORGANIZATION NAMES AND ADDRESSES Purdue University Young Hall 155 South Grant Street West Lafayette, IN 47907 -2114	8. PERFORMING ORGANIZATION REPORT NUMBER
---	--

9. SPONSORING/MONITORING AGENCY NAME(S) AND ADDRESS (ES) U.S. Army Research Office P.O. Box 12211 Research Triangle Park, NC 27709-2211	10. SPONSOR/MONITOR'S ACRONYM(S) ARO
	11. SPONSOR/MONITOR'S REPORT NUMBER(S) 65957-PH-II.1

12. DISTRIBUTION AVAILABILITY STATEMENT Approved for Public Release; Distribution Unlimited
--

13. SUPPLEMENTARY NOTES The views, opinions and/or findings contained in this report are those of the author(s) and should not be construed as an official Department of the Army position, policy or decision, unless so designated by other documentation.

14. ABSTRACT The rigorous development of an electromagnetic force density expression is pursued along various lines. Based on experimental evidence, we suggest that a single formulation may describe forces on homogenized materials. That expression is consistent with a development attributed to Einstein and Laub. Supporting theory that was evidently unknown allows an interpretation in the static limit that agrees with the work of Lorentz. While there remain aspects related to material response that cannot currently be evaluated because of a lack of experimental data, carefully

15. SUBJECT TERMS Optical force theory; Electromagnetics

16. SECURITY CLASSIFICATION OF:			17. LIMITATION OF ABSTRACT UU	15. NUMBER OF PAGES	19a. NAME OF RESPONSIBLE PERSON Kevin Webb
a. REPORT UU	b. ABSTRACT UU	c. THIS PAGE UU			19b. TELEPHONE NUMBER 765-494-3373

Report Title

Final Report: Optical Force Theory

ABSTRACT

The rigorous development of an electromagnetic force density expression is pursued along various lines. Based on experimental evidence, we suggest that a single formulation may describe forces on homogenized materials. That expression is consistent with a development attributed to Einstein and Laub. Supporting theory that was evidently unknown allows an interpretation in the static limit that agrees with the work of Lorentz. While there remain aspects related to material response that cannot currently be evaluated because of a lack of experimental data, carefully conceived theoretical and experimental work will allow complete verification or form a basis for a revised theory. Following more than one century of effort, it appears we are close to a complete description of the mechanical aspects of the interaction of electromagnetic waves with matter. Additional research contributions related to optical forces are summarized. Specifically, we propose that the pressure on a surface in vacuum can be increased based on structure and composition.

Enter List of papers submitted or published that acknowledge ARO support from the start of the project to the date of this printing. List the papers, including journal references, in the following categories:

(a) Papers published in peer-reviewed journals (N/A for none)

<u>Received</u>	<u>Paper</u>
-----------------	--------------

TOTAL:

Number of Papers published in peer-reviewed journals:

(b) Papers published in non-peer-reviewed journals (N/A for none)

<u>Received</u>	<u>Paper</u>
-----------------	--------------

TOTAL:

Number of Papers published in non peer-reviewed journals:

(c) Presentations

Number of Presentations: 0.00

Non Peer-Reviewed Conference Proceeding publications (other than abstracts):

Received Paper

TOTAL:

Number of Non Peer-Reviewed Conference Proceeding publications (other than abstracts):

Peer-Reviewed Conference Proceeding publications (other than abstracts):

Received Paper

TOTAL:

Number of Peer-Reviewed Conference Proceeding publications (other than abstracts):

(d) Manuscripts

Received Paper

TOTAL:

Number of Manuscripts:

Books

Received Book

TOTAL:

Received

Book Chapter

TOTAL:

Patents Submitted

Patents Awarded

Awards

Kevin Webb - Fellow of the American Physical Society

Graduate Students

<u>NAME</u>	<u>PERCENT SUPPORTED</u>
FTE Equivalent:	
Total Number:	

Names of Post Doctorates

<u>NAME</u>	<u>PERCENT SUPPORTED</u>
FTE Equivalent:	
Total Number:	

Names of Faculty Supported

<u>NAME</u>	<u>PERCENT SUPPORTED</u>
FTE Equivalent:	
Total Number:	

Names of Under Graduate students supported

<u>NAME</u>	<u>PERCENT SUPPORTED</u>
FTE Equivalent:	
Total Number:	

Student Metrics

This section only applies to graduating undergraduates supported by this agreement in this reporting period

The number of undergraduates funded by this agreement who graduated during this period: 0.00

The number of undergraduates funded by this agreement who graduated during this period with a degree in science, mathematics, engineering, or technology fields:..... 0.00

The number of undergraduates funded by your agreement who graduated during this period and will continue to pursue a graduate or Ph.D. degree in science, mathematics, engineering, or technology fields:..... 0.00

Number of graduating undergraduates who achieved a 3.5 GPA to 4.0 (4.0 max scale):..... 0.00

Number of graduating undergraduates funded by a DoD funded Center of Excellence grant for Education, Research and Engineering:..... 0.00

The number of undergraduates funded by your agreement who graduated during this period and intend to work for the Department of Defense 0.00

The number of undergraduates funded by your agreement who graduated during this period and will receive scholarships or fellowships for further studies in science, mathematics, engineering or technology fields:..... 0.00

Names of Personnel receiving masters degrees

NAME
Total Number:

Names of personnel receiving PHDs

NAME
Total Number:

Names of other research staff

NAME PERCENT SUPPORTED
FTE Equivalent:
Total Number:

Sub Contractors (DD882)

Inventions (DD882)

Scientific Progress

Please refer to the report.

Technology Transfer

Progress Report for ARO Award W911NF-14-1-0606

Optical Force Theory

Kevin Webb Group
School of Electrical and Computer Engineering
Purdue University
West Lafayette, Indiana 47907, USA
webb@purdue.edu

Program Manager: Dr. Richard Hammond
Army Research Office

November 28, 2015

Abstract

The rigorous development of an electromagnetic force density expression is pursued along various lines. Based on experimental evidence, we suggest that a single formulation may describe forces on homogenized materials. That expression is consistent with a development attributed to Einstein and Laub. Supporting theory that was evidently unknown allows an interpretation in the static limit that agrees with the work of Lorentz. While there remain aspects related to material response that cannot currently be evaluated because of a lack of experimental data, carefully conceived theoretical and experimental work will allow complete verification or form a basis for a revised theory. Following more than one century of effort, it appears we are close to a complete description of the mechanical aspects of the interaction of electromagnetic waves with matter.

Additional research contributions related to optical forces are summarized. Specifically, we propose that the pressure on a surface in vacuum can be increased based on structure and composition. This recent Physical Review journal paper presents the idea of using a nanostructured cavity array in a gold surface at resonance and shows simulated results that motivate experimental verification. Once proven, this very substantial effect should be important in optomechanics because the relatively weak optical force can be made much larger, improving actuators. There may also be applications in solar sails for space vehicle propulsion.

Contents

1	Introduction	1
1.1	Preamble	1
1.2	Optical Forces, Radiation Pressure and Trapping	1
1.3	Maxwell's Equations	2
1.4	Description of Materials	3
1.5	Causality and Material Response	4
1.6	Conservation of Energy	4
2	Lorentz Force	5
2.1	Lorentz Force for Static Fields	5
2.2	Generalization of Lorentz Force	6
3	Kinetic and electromagnetic Momentum	7
3.1	Conservation of Kinetic Momentum and Energy	7
3.2	Electromagnetic Momentum	8
3.3	Relationship Between Classical Fields and Photon Momentum	8
4	Force Theory with the Abraham Momentum	10
4.1	Electromagnetic Force Density	10
4.2	Einstein-Laub Force Expression	12
4.3	Initial Analysis of Einstein-Laub Formulation	13
4.4	A Different Minkowski Formulation	14
4.5	Other Prospects with the Abraham Momentum	15
5	Force Theory with the Minkowski Momentum	15
6	Note on $(\nabla \cdot \mathbf{P}) \mathbf{E}$ and $(\mathbf{P} \cdot \nabla) \mathbf{E}$	17
7	Lorentz Forces from Stress tensor	18
7.1	Lorentz Electrostatic Force	18
7.2	Lorentz Magnetostatic Force	18
8	Time-Averaged Force	19
9	Force from the Stress Tensor - Stress Tensor Method	20
10	Torque	22
11	Description of Experiments	23
11.1	Prediction of the Jones and Leslie Experiments	23
11.2	Prediction of Ashkin's Water Experiment	27
11.3	Prediction of Atom Recoil Momentum Experiment	33
12	Additional Contribution - Pressure Enhancement from a Structured Metal Surface	37
13	Conclusion	41

1 Introduction

1.1 Preamble

The theory of electromagnetic forces has received substantial attention during the past century [1, 2], but uncertainty remains and there have been challenges to explain the modest set of careful experiments that have been done. This leads to the need to evaluate the derivation of the force density using various paths to establish whether there is more than one legitimate approach. The goal of this research is to extend our rigorous derivation of optical forces on materials that used the Abraham momentum to consider other approaches, including use of the Minkowski momentum, along with the study of related issues in the momentum flow or stress tensor. If there should be more than one plausible approach, we will design a set of experiments that could be pursued in subsequent works to differentiate and establish correctness. This fundamental theoretical work is complemented by simulation results for various materials. For instance, we have shown that the Abraham momentum leads to the conclusion that the radiation pressure sign does not change with the sign of the refractive index. We evaluate issues with other possible formulations regarding the influence of the material properties. Also, by correctly incorporating material dispersion, forces using pulsed light can be understood. Furthermore, by exploiting nonlinear material properties, other interesting control may be possible.

There are important practical applications of this fundamental work of electromagnetic forces. While optical tweezers are becoming more common, and wonderful applications exist, particularly in molecular biology, there is little fundamental understanding of absolute force data from the calibration procedures [3, 4]. Also, optical tweezers apply a relatively weak force over large (many micron meters) length scales, leading to the need for the force to be applied to large beads. By evaluating the relation between materials and nanostructures and the force, it should be possible to design tweezers with larger forces to move smaller objects or larger objects locally. This could be important in sensing, for instance, where a molecule could be moved to a region with large field and hence large Raman dipole moment for identification. There could be new control opportunities by control of the optical material properties, both electric and magnetic, and material synthesis work could be motivated by the basic understanding we seek.

1.2 Optical Forces, Radiation Pressure and Trapping

The mathematical description of electromagnetic forces on material has received much attention during the past century or so (see, for example, [1, 5–20]), in order to describe experiments done over that time frame (notable results being [21, 22]). Understanding the force due to electromagnetic fields is fundamental and of importance in applications like optical tweezers [23, 24] and the study of optical traps [25]. While a propagating uniform electromagnetic plane wave in vacuum has been assumed to apply a positive force and radiation pressure, recent investigations have suggested that this situation may change when the fields are in a negative refractive index medium [12, 26–28]. In our earlier work, we showed that the force density is positive for propagating waves in passive homogeneous media, even when the refractive index is negative, and that a material offering gain can produce a negative force [16, 17]. Treatment of the electromagnetic force on a dielectric slab has indicated that the interfaces influence the force density [9], except in the case of incidence at the Brewster angle [29]. Numerical models for electromagnetic pulses in lossless and lossy positive and negative refractive index slabs [18] and semi-infinite media [30] appear to have similar force behavior. However, the impact of the material parameters of the background and the slab on the electromagnetic force density in the slab has remained unclear. Also, any force experiment with gain

material must involve finite material extent, and the force behavior in a slab having overall gain is not known.

Two oppositely charged surfaces are attracted because of the electrostatic force, as presented by Coulomb. Parallel wires carrying currents in opposite directions have an attractive force. These forces have been described by Lorentz in vacuum as $\mathbf{F} = q\mathbf{E} + q\mathbf{v} \times \mu_0\mathbf{H}$, or equivalently, in terms of the energies in the electrostatic (u_E) and magnetostatic (u_H) fields, resulting in $\mathbf{F} = \pm\nabla W|_p$, with p indicating constant charge or potential (or flux or current for the magnetic case), which dictates the sign. The quantum field also gives rise to a (Casimir) force between uncharged surfaces in vacuum that is attractive [31]. Generally, forces can be decomposed into a gradient or dipole force associated with a spatially varying field, as used in optical tweezers [23, 24], and that due to radiation pressure involving atomic transitions [21]. Evanescent fields between two surfaces or waveguides can result in a force due to the modal electric field perpendicular to the two surfaces or waveguides, which gives rise to attraction and a polarization charge having opposite sign, or repulsion with the mode of opposite symmetry, i.e., forces dictated by the direction of the associated electric fields, thereby being examples of dipole forces [32].

The radiation pressure is related to a change in momentum (between incident and emitted photons), and all experimental evidence suggests that this results in a force in the direction of the incident field momentum (Poynting vector and wave vector). While a propagating uniform electromagnetic plane wave in vacuum has been assumed to apply a positive force and radiation pressure, recent investigations have suggested that this situation may change when the fields are in a negative refractive index medium [12, 26, 27, 33]. We consider the various contributors to the electromagnetic force, including the material constitutive parameters and their dispersive properties. This analysis indicates that the radiation pressure is positive for propagating waves in passive homogeneous media, even when the refractive index is negative. In earlier work, we proposed that a homogeneous material with gain can result in a negative force [16]. Here, we study the various contributors to the force in dispersive materials, and provide a detailed description of an experiment to demonstrate a negative force in a gain medium. We also describe a negative force for the case of evanescent fields, even when there is no electric field component in that direction.

There has been much work done related to the description of forces due to electromagnetic waves (see [6–8, 10, 11, 34, 35], for example) and accurate measurements [22]. We note that there have been some issues in interpreting all measurements (notably with a non-unity background refractive index [22]), which has led to debate on use of the Abraham versus the Minkowski momentum definition. Many have used a rigorous force development from Maxwell’s equations that employs the Abraham form [6–8, 10, 11, 16, 34].

1.3 Maxwell’s Equations

Maxwell’s equations with SI units are commonly written [36]

$$\nabla \times \mathbf{E} = -\frac{\partial \mathbf{B}}{\partial t} \quad [\text{Faraday}] \quad (1)$$

$$\nabla \times \mathbf{H} = \frac{\partial \mathbf{D}}{\partial t} + \mathbf{J} \quad [\text{Ampere}] \quad (2)$$

$$\nabla \cdot \mathbf{D} = \rho \quad [\text{Gauss – electric}] \quad (3)$$

$$\nabla \cdot \mathbf{B} = 0 \quad [\text{Gauss – magnetic}], \quad (4)$$

where \mathbf{E} is the electric field (V/m), \mathbf{H} is the magnetic field (A/m), \mathbf{D} is the electric flux density (C/m²), \mathbf{B} is the magnetic flux density (T=Wb/m²), \mathbf{J} is the electric current density (A/m²), and ρ is the electric charge density (C/m³).

Taking the divergence of (2) and substituting (3) gives

$$\nabla \cdot \mathbf{J} = -\frac{\partial \rho}{\partial t}. \quad (5)$$

Equation (5) is the continuity equation, stating that (classically) charge is conserved - and simply moved around.

With $\exp(-i\omega t)$, $\partial/\partial t \rightarrow -i\omega$ [$\exp(j\omega t)$, $\partial/\partial t \rightarrow j\omega$], (1) - (4) become

$$\nabla \times \mathbf{E} = i\omega \mathbf{B} \quad (6)$$

$$\nabla \times \mathbf{H} = -i\omega \mathbf{D} + \mathbf{J} \quad (7)$$

$$\nabla \cdot \mathbf{D} = \rho \quad (8)$$

$$\nabla \cdot \mathbf{B} = 0. \quad (9)$$

1.4 Description of Materials

Bi-anisotropic materials can be described by constitutive relations of the form [37]

$$\mathbf{D} = \epsilon_0 \bar{\epsilon} \cdot \mathbf{E} + i\sqrt{\mu_0 \epsilon_0} \bar{\kappa}^T \cdot \mathbf{H} \quad (10)$$

$$\mathbf{B} = -i\sqrt{\mu_0 \epsilon_0} \bar{\kappa} \cdot \mathbf{E} + \mu_0 \bar{\mu} \cdot \mathbf{H}, \quad (11)$$

where $\bar{\epsilon}$ is the dielectric constant tensor, $\bar{\mu}$ is the relative permeability tensor, and $\bar{\kappa}$ is the chiral tensor.

For simple, isotropic media, (10) and (11), become

$$\mathbf{D} = \epsilon_0 \epsilon \mathbf{E} \quad (12)$$

$$\mathbf{B} = \mu_0 \mu \mathbf{H}. \quad (13)$$

We assume complex material parameters in the frequency domain of the form

$$\epsilon = \epsilon' + i\epsilon'' \quad (14)$$

$$\mu = \mu' + i\mu''. \quad (15)$$

Ohm's Law is

$$\mathbf{J} = \sigma \mathbf{E} \quad (16)$$

$$\sigma = \sigma' + i\sigma'', \quad (17)$$

where σ is the complex conductivity. Ampere's Law becomes

$$\nabla \times \mathbf{H} = -i\omega \epsilon_0 \epsilon \mathbf{E} + \mathbf{J}_i \quad (18)$$

$$= \sigma \mathbf{E} + \mathbf{J}_i, \quad (19)$$

where \mathbf{J}_i is some source (impressed) current density and it is clear that ϵ and σ carry equivalent information about the electric material response.

1.5 Causality and Material Response

In the frequency domain, with an isotropic material response, $\mathbf{D}(\mathbf{r}, \omega) = \epsilon(\omega)\epsilon_0\mathbf{E}(\mathbf{r}, \omega)$ leading to the local in space and nonlocal in time convolution in the time domain,

$$\mathbf{D}(\mathbf{r}, t) = \int_{-\infty}^{\infty} \epsilon(t')\epsilon_0\mathbf{E}(\mathbf{r}, t - t')dt'. \quad (20)$$

Using the electric susceptibility, $\chi_E(\omega) = \epsilon(\omega) - 1$,

$$\chi_E(t) = \frac{1}{2\pi} \int_{-\infty}^{\infty} [\epsilon(\omega) - 1] e^{-i\omega t} d\omega. \quad (21)$$

$$\epsilon = 1 + \int_{t_r}^{\infty} \chi_E(t) e^{i\omega t} dt \quad (22)$$

A two-level atomic system has

$$\chi_E = \epsilon - 1 \quad (23)$$

$$= \frac{\omega_p^2}{\omega_0^2 - \omega^2 - i2\gamma\omega} \quad (24)$$

In the case where the local atom is a distance r from the source that turns on at $t = 0$, the field arrives at a retarded time $t_r = r/v$, with $v = c$ (regardless of the material composition). We set $t_r = 0$, and hence assume that $\chi_E(t) = 0$ for $t < 0$, leading to

$$\int_{-\infty}^{\infty} [\epsilon(\omega) - 1] e^{-i\omega t} d\omega = 0 \quad (25)$$

Assuming analyticity in upper half of $\omega = \omega' + i\omega''$ plane [36, 38, 39]

$$\oint \frac{\epsilon(\omega) - 1}{\omega' - \omega} d\omega' = 0 \quad (26)$$

Evaluating the integral in (26) in the complex plane gives the Kramers-Kronig relations (Hilbert transform pair) [36, 39]

$$\epsilon'(\omega) - 1 = \frac{2}{\pi} \int_0^{\infty} \frac{\omega' \epsilon''(\omega')}{\omega'^2 - \omega^2} d\omega' \quad (27)$$

$$\epsilon''(\omega) = -\frac{2\omega}{\pi} \int_0^{\infty} \frac{\epsilon'(\omega') - 1}{\omega'^2 - \omega^2} d\omega', \quad (28)$$

where the symmetry to make $\epsilon(t)$ real has been assumed and the singularity evaluated, hence the principal value integral.

1.6 Conservation of Energy

The vector identity

$$\nabla \cdot (\mathbf{E} \times \mathbf{H}) = \mathbf{H} \cdot \nabla \times \mathbf{E} - \mathbf{E} \cdot \nabla \times \mathbf{H}, \quad (29)$$

together with Maxwell's curl equations,

$$\nabla \times \mathbf{E} = -\frac{\partial \mathbf{B}}{\partial t} \quad (30)$$

$$\nabla \times \mathbf{H} = \frac{\partial \mathbf{D}}{\partial t}, \quad (31)$$

leads to Poynting's theorem [36]

$$\oint \mathbf{E} \times \mathbf{H} \cdot d\mathbf{s} = - \int \left[\mathbf{E} \cdot \frac{\partial \mathbf{D}}{\partial t} + \mathbf{H} \cdot \frac{\partial \mathbf{B}}{\partial t} \right] dv. \quad (32)$$

From (32),

$$\frac{\partial u}{\partial t} = \mathbf{E} \cdot \frac{\partial \mathbf{D}}{\partial t} + \mathbf{H} \cdot \frac{\partial \mathbf{B}}{\partial t}, \quad (33)$$

where u is the energy density in the electric and magnetic fields.

We assume that (32) describes electromagnetic energy and power flow in all experiments, and it appears to have been used effectively for a very long time. For example, application of the boundary conditions on tangential fields at an interface between two materials enforces the continuity of tangential fields, under the assumption that there is no surface current density, and hence conservation of energy by applying (32) at this field continuity condition.

2 Lorentz Force

2.1 Lorentz Force for Static Fields

Lorentz described the forces on charges as [5]

$$\mathbf{F} = q\mathbf{E} + q\mathbf{v} \times \mathbf{B}, \quad (34)$$

but his focus was vacuum so that this expression becomes

$$\mathbf{F} = q\mathbf{E} + q\mathbf{v} \times \mu_0\mathbf{H}, \quad (35)$$

where \mathbf{v} is the instantaneous velocity of the (point) charge q . Note that the component due to the electric field ($q\mathbf{E}$) comes directly from the definition of the electrostatic field and that the magnetic field term relates to the observed cyclotron motion of charges in a magnetic field ($q\mathbf{v} \times \mu_0\mathbf{H}$). The magnetic field term is most often written as $\mathbf{v} \times \mathbf{B}$, but Lorentz's use was in vacuum, where for SI units, $\mathbf{B} = \mu_0\mathbf{H}$. An important question is whether (34) or (35) is correct in magnetic media.

The question as to whether $q\mathbf{v} \times \mathbf{B}$ or $q\mathbf{v} \times \mu_0\mathbf{H}$ should be used has been controversial. It has been suggested that experiments lead to the conclusion that as $v \rightarrow c$, (34) applies [39] (see page 144). However, this argument essentially says that small velocities relate to random electron motion with little influence of the magnetic medium, hence avoiding the central question. Electron microscopy has been used to determine the distribution of magnetism [40], and those experiments support use of magnetization \mathbf{M} and indicate that in the situations considered the applied field (\mathbf{H}) was unimportant. While early experiments gave conflicting pictures [41] (see the introduction), an experiment showing the deflection of mesons by magnetized iron suggests that \mathbf{B} is the correct vector [41]. The measurement method became known as Lorentz microscopy, which is sensitive to magnetized material states [42, 43]. *Therefore, experimental evidence to date appears to support use of (34).*

2.2 Generalization of Lorentz Force

From (34), the force density is

$$\mathbf{f} = \rho \mathbf{E} + \mathbf{J} \times \mathbf{B}. \quad (36)$$

Consider a generalization of (36). From Gauss's law (3), writing $\mathbf{D} = \epsilon_0 \mathbf{E} + \mathbf{P}$, with \mathbf{P} the polarization vector, the total electric charge density is

$$\begin{aligned} \rho_t &= \epsilon_0 \nabla \cdot \mathbf{E} \\ &= \nabla \cdot \mathbf{D} - \nabla \cdot \mathbf{P} \\ &= \rho - \nabla \cdot \mathbf{P}. \end{aligned} \quad (37)$$

Likewise from (4) for the magnetic field, assuming $\mathbf{B} = \mu_0 (\mathbf{H} + \mathbf{M})$, with \mathbf{M} the magnetization,

$$\begin{aligned} \rho_{mt} &= \mu_0 \nabla \cdot \mathbf{H} \\ &= \nabla \cdot \mathbf{B} - \mu_0 \nabla \cdot \mathbf{M} \\ &= 0 - \mu_0 \nabla \cdot \mathbf{M}. \end{aligned} \quad (38)$$

In (38), $\nabla \cdot \mathbf{M}$ corresponds to the magnetic moment charge density (associated with the spin and orbital angular momentum).

From Ampere's law (2)

$$\begin{aligned} \nabla \times \mathbf{H} &= \frac{1}{\mu_0} \nabla \times \mathbf{B} - \nabla \times \mathbf{M} \\ &= \frac{\partial \mathbf{D}}{\partial t} + \mathbf{J}. \end{aligned} \quad (39)$$

Rearranging gives the total current density as

$$\begin{aligned} \nabla \times \frac{\mathbf{B}}{\mu_0} &= \left(\nabla \times \mathbf{M} + \frac{\partial \mathbf{D}}{\partial t} + \mathbf{J} \right) \\ &= \mathbf{J}_{mt} + \mathbf{J}_t + \epsilon_0 \frac{\partial \mathbf{E}}{\partial t}. \end{aligned} \quad (40)$$

Note that classical, static magnetism is viewed as the motion of bound electric charge, so that we might consider insertion of both electric and magnetic charges and currents into (36). Proceeding with this gives

$$\boxed{\mathbf{f}_L = (\rho - \nabla \cdot \mathbf{P} - \mu_0 \nabla \cdot \mathbf{M}) \mathbf{E} + \left(\nabla \times \mathbf{M} + \frac{\partial \mathbf{P}}{\partial t} + \mathbf{J} \right) \times \mathbf{B},} \quad (41)$$

where we have taken the liberty to call this a Lorentz force. With the removal of the magnetic material terms in (41), we have

$$\mathbf{f}_{LE} = (\rho - \nabla \cdot \mathbf{P}) \mathbf{E} + \left(\frac{\partial \mathbf{P}}{\partial t} + \mathbf{J} \right) \times \mathbf{B}, \quad (42)$$

where $\mathbf{B} = \mu_0 \mathbf{H}$. There is no *a priori* reason to believe that (41) or (42) should be correct, and there is no direct relation to photon momentum. However, in the limit that the static situation is approached, one would expect those physics to apply. In the special case of electric materials, the form in (42) has been presented previously [44, 45].

3 Kinetic and electromagnetic Momentum

3.1 Conservation of Kinetic Momentum and Energy

The conservation of kinetic momentum is described by [6]

$$\nabla \cdot \mathbf{T}_k + \frac{\partial \mathbf{g}_k}{\partial t} = \mathbf{f}_k, \quad (43)$$

where \mathbf{T} is the kinetic momentum flow tensor or the stress tensor, \mathbf{g}_k is the kinetic momentum, with $\mathbf{g}_k = \rho_m \mathbf{v}$, where ρ_m is the mass density.

The conservation of kinetic energy is described by [6]

$$\nabla \cdot \mathbf{S}_k + \frac{\partial u_k}{\partial t} = \phi_k. \quad (44)$$

For the case of the electromagnetic component, $\mathbf{S}_k \rightarrow \mathbf{S}_e$ and $u_k \rightarrow u_e$. Comparing (44) with Poynting's theorem in (32), and with the inclusion of impressed current \mathbf{J}_i in Ampere's law, results in

$$\mathbf{S}_e = \mathbf{E} \times \mathbf{H} \quad (45)$$

$$u_e = \mathbf{E} \cdot \frac{\partial \mathbf{D}}{\partial t} + \mathbf{H} \cdot \frac{\partial \mathbf{B}}{\partial t} \quad (46)$$

$$\phi_e = -\mathbf{E} \cdot \mathbf{J}_i. \quad (47)$$

A closed electromagnetic and kinetic system would satisfy [6]

$$\begin{aligned} \nabla \cdot (\mathbf{T}_k + \mathbf{T}_e) + \frac{\partial}{\partial t} (\mathbf{g}_k + \mathbf{g}_e) &= \mathbf{f}_k + \mathbf{f}_e \\ &= 0, \end{aligned} \quad (48)$$

and

$$\begin{aligned} \nabla \cdot (\mathbf{S}_k + \mathbf{S}_e) + \frac{\partial}{\partial t} (u_k + u_e) &= \phi_e + \phi_k \\ &= 0. \end{aligned} \quad (49)$$

Note that there is a power conversion efficiency that transfers power between the charges (ϕ_k) and the electromagnetic field (ϕ_e). Also, (48) implies

$$\mathbf{f}_k = -\mathbf{f}_e = -\left(\nabla \cdot \mathbf{T}_e + \frac{\partial \mathbf{g}_e}{\partial t} \right), \quad (50)$$

a result we will use.

The term ‘‘virtual power’’ has been used by Penfield and Haus to describe coupled physical systems [6]. For example, with interacting electromagnetic and thermodynamic (subscript h for heat) systems,

$$\mathbf{f}_e + \mathbf{f}_h + \mathbf{f}_k = 0 \quad (51)$$

$$\phi_e + \phi_h + \phi_k = 0, \quad (52)$$

from which a revised force theory can be formed. This leads to the need to understand the systems involved and to present a suitable mathematical description within a framework such as this.

3.2 Electromagnetic Momentum

The Abraham form of the electromagnetic momentum density is [46, 47]

$$\mathbf{g}_A = \frac{1}{c^2} \mathbf{E} \times \mathbf{H}, \quad (53)$$

with c the speed of light in vacuum. For electromagnetic energy in nondispersive media, this yields the single photon momentum magnitude of $\hbar k_0/n$, where n is refractive index, $\hbar = h/2\pi$, with h being Planck's constant, and k_0 is the free space wave number. Doing likewise with the Minkowski momentum density [48, 49]

$$\mathbf{g}_M = \mathbf{D} \times \mathbf{B} \quad (54)$$

gives a momentum of $n\hbar k_0$ in the simplified situation where the refractive index is a real quantity. Atoms have been measured to have a recoil momentum of $n\hbar k_0$ [25], important in atom interferometry with optical gratings and consistent with the deBroglie momentum. In vacuum, of course, $\mathbf{g}_A = \mathbf{g}_M$. Therefore, the issue is how to treat (or partition) momentum and force within homogenized material.

A key point in the assignment of an electromagnetic momentum is the coupling of various physical systems and the fact that conservation principles apply to the superposition of these. This has been treated nicely with a virtual power concept [6], which provides basic insight into the separation of mechanical and electromagnetic effects [7]. The delineation into a quantum mechanical canonical momentum that produces spatial translations [50] and kinetic momenta associated with Abraham or Minkowski have been proposed [51, 52]. However, it has been noted that only the (dispersionless) canonical momentum of the photon appears to explain the Jones and Leslie experiments [51]. Of general significance, the influence of dispersion must be incorporated to determine the momentum imparted [53]. At this point, the Jones and Leslie radiation pressure experiments [22] remain unexplained, except for the qualitative similarity to the photon momentum. More generally, there remain basic questions about how to describe electromagnetic forces in dispersive materials, or more specifically, whether current descriptions can explain experiments.

We showed that an interpretation of the resulting force expression that incorporates the Abraham momentum can explain the dependence of the radiation pressure on refractive index in the experiments of Jones and Leslie [54]. This picture was expanded to describe why Jones and Leslie concluded from their experiments that there was no dependence of the force on polarization or angle of incidence [22]. While it has been noted that the Abraham momentum fails to predict the Jones and Leslie results [51], the analysis here shows that the Abraham momentum incorporated into a general force expression explains these experiments. Importantly, this model could be used to predict other force results, whereas the observation that the near-normal incidence results from Jones and Leslie are consistent with the incident photons carrying a canonical momentum of $n\hbar k_0$ [51], while appealing, cannot directly be applied to determine electromagnetic forces. Likewise, the separation of the photon momentum into canonical (identified as Abraham) and kinetic (identified as Minkowski) momenta [52] does not provide a description for force. Other work has investigated issues surrounding the Jones and Leslie experiments, including the force on a perfect conductor in a background medium [55], and that on other materials as being due to the impedance mismatch [56, 57]. This leads to the primary contribution summarized here, the explanation of all experimental results obtained by Jones and Leslie for the first time and using a rigorous and general force model stemming from Maxwell's equations with homogenized material parameters.

3.3 Relationship Between Classical Fields and Photon Momentum

We review the development of the photon momenta associated with (53) and (54) for tutorial reasons and also because the assumptions, namely that dispersion and loss in the atomic/material response

are ignored. This development by and large follows an earlier review [58].

From (32), Poynting's theorem, and in vacuum,

$$\frac{\partial u_0}{\partial t} = \epsilon_0 \mathbf{E} \cdot \frac{\partial \mathbf{E}}{\partial t} + \mu_0 \mathbf{H} \cdot \frac{\partial \mathbf{H}}{\partial t}. \quad (55)$$

Ignoring the spatial dependence and for a monochromatic plane wave, we set $\mathbf{E} = \hat{\mathbf{e}} E_0 \cos(\omega t)$ and $\mathbf{H} = \hat{\mathbf{h}} (E_0/\eta_0) \cos(\omega t)$, where the free space wave impedance is $\eta_0 = \sqrt{\mu_0/\epsilon_0}$, and the energy density can be written from (55) as

$$\begin{aligned} u_0(t) &= \frac{1}{2} \epsilon_0 E^2 + \frac{1}{2} \mu_0 H^2 \\ &= \epsilon_0 E^2. \end{aligned} \quad (56)$$

The free space momentum density is

$$\begin{aligned} \mathbf{g}_0 &= \frac{1}{c^2} \mathbf{E} \times \mathbf{H} \\ &= \hat{\mathbf{e}} \times \hat{\mathbf{h}} \frac{\epsilon_0 E^2}{c} \end{aligned} \quad (57)$$

From the instantaneous momentum density in (57) we write the peak value as

$$g_{0p} = \frac{\epsilon_0 E_0^2}{c} \quad (58)$$

From (56), the photon energy is written as

$$\hbar\omega = u_{0p} = \epsilon_0 E_0^2, \quad (59)$$

and from (56) with substitution of the photon momentum (p_0) for g_0 , we have

$$E_0^2 = \frac{\hbar\omega}{\epsilon_0} = \frac{p_0 c}{\epsilon_0}. \quad (60)$$

Equation (60) gives the vacuum photon momentum as

$$p_0 = \hbar k_0, \quad (61)$$

with $k_0 = \omega/c$ the free space wave number, in accordance with quantum theory [50].

Consider now the situation in a dielectric with refractive index $n = \sqrt{\epsilon}$. *Neglecting dispersion* (the frequency dependence of the dielectric constant and loss), the energy density becomes

$$u = \frac{1}{2} (\epsilon_0 \mathbf{D} \cdot \mathbf{E} + \mu_0 \mathbf{B} \cdot \mathbf{H}). \quad (62)$$

If we consider the dielectric constant real and independent of frequency, we have $\mathbf{D}(t) = \epsilon_0 \epsilon \mathbf{E}(t)$ and $\mathbf{H} = \hat{\mathbf{h}} (E_0/\eta) \cos(\omega t)$, with $\eta = \eta_0/\sqrt{\epsilon}$. The Minkowski momentum density is

$$\begin{aligned} \mathbf{g}_M &= \mathbf{D} \times \mathbf{B} \\ &= \hat{\mathbf{e}} \times \hat{\mathbf{h}} \frac{E^2 \epsilon_0 \epsilon^{3/2}}{c}. \end{aligned} \quad (63)$$

The peak momentum density is

$$g_{Mp} = \frac{E_0^2 \epsilon_0 \epsilon^{3/2}}{c}. \quad (64)$$

Using a procedure similar to that to obtain (59),

$$\hbar\omega = u_p = \epsilon_0 \epsilon E_0^2. \quad (65)$$

Substituting the Minkowski photon momentum (p_M) for g_{Mp} in (64), we have

$$E_0^2 = \frac{\hbar\omega}{\epsilon_0 \epsilon} = \frac{p_M c}{\epsilon_0 \epsilon n}, \quad (66)$$

with n the refractive index, written this way because it is retained, from which we have

$$p_M = \hbar k_0 n. \quad (67)$$

A similar procedure with the Abraham momentum yields

$$\begin{aligned} \mathbf{g}_A &= \frac{1}{c^2} \mathbf{E} \times \mathbf{H} \\ &= \hat{\mathbf{e}} \times \hat{\mathbf{h}} \frac{E^2}{c^2 \eta} \\ &= \hat{\mathbf{e}} \times \hat{\mathbf{h}} \frac{E^2 \epsilon_0 n}{c}. \end{aligned} \quad (68)$$

Equating energies gives

$$\hbar\omega = u_p = \epsilon_0 \epsilon E_0^2, \quad (69)$$

and hence

$$E_0^2 = \frac{\hbar\omega}{\epsilon_0 \epsilon} = \frac{p_A c}{\epsilon_0 n}, \quad (70)$$

with p_A the Abraham photon momentum. Therefore,

$$p_A = \frac{\hbar k_0}{n}. \quad (71)$$

These photon momentum were associated with field-based momentum densities in the previous section.

4 Force Theory with the Abraham Momentum

4.1 Electromagnetic Force Density

Maxwell's equations with all source terms on the right-hand side can be written

$$\nabla \times \mathbf{E} + \mu_0 \frac{\partial \mathbf{H}}{\partial t} = -\mu_0 \frac{\partial \mathbf{M}}{\partial t} \quad (72)$$

$$\nabla \times \mathbf{H} - \epsilon_0 \frac{\partial \mathbf{E}}{\partial t} = \frac{\partial \mathbf{P}}{\partial t} + \mathbf{J} \quad (73)$$

$$\epsilon_0 \nabla \cdot \mathbf{E} = -\nabla \cdot \mathbf{P} + \rho \quad (74)$$

$$\nabla \cdot \mathbf{H} = -\nabla \cdot \mathbf{M}, \quad (75)$$

with \mathbf{E} the electric field, \mathbf{H} the magnetic field, \mathbf{P} the polarization, \mathbf{M} the magnetization, \mathbf{J} the source electric current density, ρ the free electric charge density, μ_0 the permeability of free space, and ϵ_0 the permittivity of free space. Note that material dispersion and loss are incorporated into the polarization and magnetization through the frequency domain representation for these quantities. Also, any anisotropic, linear material response can be represented in this form. Taking the cross product of $\epsilon_0\mathbf{E}$ with (72) and $\mu_0\mathbf{H}$ with (73), and adding the resulting equations, gives

$$\begin{aligned} \epsilon_0\mathbf{E} \times (\nabla \times \mathbf{E}) + \mu_0\mathbf{H} \times (\nabla \times \mathbf{H}) &+ \mu_0\epsilon_0\mathbf{E} \times \frac{\partial\mathbf{H}}{\partial t} - \mu_0\epsilon_0\mathbf{H} \times \frac{\partial\mathbf{E}}{\partial t} \\ &= -\mu_0\epsilon_0\mathbf{E} \times \frac{\partial\mathbf{M}}{\partial t} + \mu_0\mathbf{H} \times \frac{\partial\mathbf{P}}{\partial t} + \mu_0\mathbf{H} \times \mathbf{J}. \end{aligned} \quad (76)$$

The momentum-flow or stress tensor for the electromagnetic field is [6]

$$\mathbf{T}_e = \frac{1}{2} (\epsilon_0 E^2 + \mu_0 H^2) \mathbf{I} - \epsilon_0 \mathbf{E}\mathbf{E} - \mu_0 \mathbf{H}\mathbf{H}, \quad (77)$$

where, for example, $\mathbf{E}\mathbf{E}$ is a dyadic product of two vectors with elements $(\mathbf{ab})_{ij} = a_i b_j$ [6]. We note that the stress tensor in (77) is symmetric [6]. A basic premise has been proposed whereby a rectangular solid under surface stress should have a symmetric stress tensor [39] (page 103). However, a more complete picture would be the superposition of all coupled systems, and a pragmatic position would suggest that arriving at the correct (or a useful) force density should be the primary concern [6].

The triple cross product terms in (76) can therefore be expressed as

$$\epsilon_0\mathbf{E} \times (\nabla \times \mathbf{E}) + \mu_0\mathbf{H} \times (\nabla \times \mathbf{H}) = \nabla \cdot \mathbf{T}_e + \epsilon_0 (\nabla \cdot \mathbf{E}) \mathbf{E} + \mu_0 (\nabla \cdot \mathbf{H}) \mathbf{H}. \quad (78)$$

Here, the divergence of the tensor in the (x_1, x_2, x_3) coordinate system is defined as

$$\nabla \cdot \mathbf{T} = \begin{bmatrix} \frac{\partial T_{11}}{\partial x_1} + \frac{\partial T_{21}}{\partial x_2} + \frac{\partial T_{31}}{\partial x_3} \\ \frac{\partial T_{12}}{\partial x_1} + \frac{\partial T_{22}}{\partial x_2} + \frac{\partial T_{32}}{\partial x_3} \\ \frac{\partial T_{13}}{\partial x_1} + \frac{\partial T_{23}}{\partial x_2} + \frac{\partial T_{33}}{\partial x_3} \end{bmatrix} \quad (79)$$

and, for example,

$$\mathbf{E}\mathbf{E} = \begin{bmatrix} E_1^2 & E_1 E_2 & E_1 E_3 \\ E_2 E_1 & E_2^2 & E_2 E_3 \\ E_3 E_1 & E_3 E_2 & E_3^2 \end{bmatrix}. \quad (80)$$

Substituting (78) into (76) gives

$$\begin{aligned} \nabla \cdot \mathbf{T}_e + \epsilon_0 (\nabla \cdot \mathbf{E}) \mathbf{E} + \mu_0 (\nabla \cdot \mathbf{H}) \mathbf{H} &= -\mu_0\epsilon_0\mathbf{E} \times \frac{\partial\mathbf{H}}{\partial t} + \mu_0\epsilon_0\mathbf{H} \times \frac{\partial\mathbf{E}}{\partial t} \\ &- \mu_0\epsilon_0\mathbf{E} \times \frac{\partial\mathbf{M}}{\partial t} + \mu_0\mathbf{H} \times \frac{\partial\mathbf{P}}{\partial t} + \mu_0\mathbf{H} \times \mathbf{J}. \end{aligned} \quad (81)$$

Taking the Abraham form of the momentum density associated with the electromagnetic field [6],

$$\mathbf{g}_A = \mathbf{g}_e = \mu_0\epsilon_0\mathbf{E} \times \mathbf{H}, \quad (82)$$

leads to

$$\frac{\partial \mathbf{g}_e}{\partial t} = \mu_0 \epsilon_0 \mathbf{E} \times \frac{\partial \mathbf{H}}{\partial t} - \mu_0 \epsilon_0 \mathbf{H} \times \frac{\partial \mathbf{E}}{\partial t}. \quad (83)$$

Using (78) and (83), (76) can re-written as

$$\nabla \cdot \mathbf{T}_e + \epsilon_0 (\nabla \cdot \mathbf{E}) \mathbf{E} + \mu_0 (\nabla \cdot \mathbf{H}) \mathbf{H} + \frac{\partial \mathbf{g}_e}{\partial t} = -\mu_0 \epsilon_0 \mathbf{E} \times \frac{\partial \mathbf{M}}{\partial t} + \mu_0 \mathbf{H} \times \frac{\partial \mathbf{P}}{\partial t} + \mu_0 \mathbf{H} \times \mathbf{J}. \quad (84)$$

The kinetic force density due to the electromagnetic fields, or the conservation of momentum (density), can now be written in terms of \mathbf{T}_e and \mathbf{g}_e as

$$\mathbf{f} = -\mathbf{f}_e \quad (85)$$

$$\equiv \mathbf{f}_E \quad (86)$$

$$\begin{aligned} &= -\nabla \cdot \mathbf{T}_e - \frac{\partial \mathbf{g}_e}{\partial t} \\ &= \mu_0 \epsilon_0 \mathbf{E} \times \frac{\partial \mathbf{M}}{\partial t} - \mu_0 \mathbf{H} \times \frac{\partial \mathbf{P}}{\partial t} + \epsilon_0 (\nabla \cdot \mathbf{E}) \mathbf{E} + \mu_0 (\nabla \cdot \mathbf{H}) \mathbf{H} - \mu_0 \mathbf{H} \times \mathbf{J}. \end{aligned} \quad (87)$$

Substituting (74) and (75) into (87) gives

$$\boxed{\mathbf{f}_E = \frac{\partial \mathbf{P}}{\partial t} \times \mu_0 \mathbf{H} - \frac{\partial \mathbf{M}}{\partial t} \times \mu_0 \epsilon_0 \mathbf{E} - (\nabla \cdot \mathbf{P}) \mathbf{E} + \rho \mathbf{E} - \mu_0 (\nabla \cdot \mathbf{M}) \mathbf{H} - \mu_0 \mathbf{H} \times \mathbf{J},} \quad (88)$$

Writing (88) for free space,

$$\mathbf{f} = \epsilon_0 (\nabla \cdot \mathbf{E}) \mathbf{E} - \mu_0 (\nabla \cdot \mathbf{H}) \mathbf{H} - \mu_0 \mathbf{H} \times \mathbf{J}. \quad (89)$$

Substituting (3) and (4) gives

$$\mathbf{f} = \rho \mathbf{E} + \mathbf{J} \times \mu_0 \mathbf{H}, \quad (90)$$

which is the Lorentz force density in (35). This provides both a reference and some confidence in the development, at least for the free space case.

4.2 Einstein-Laub Force Expression

In an open system, partner polarization and magnetization charges outside the (differential) volume would produce additional forces [6]. Substituting $\epsilon_0 (\nabla \cdot \mathbf{E})$ and $\nabla \cdot \mathbf{H}$ from (74) and (75) into (87), using

$$-(\nabla \cdot \mathbf{P}) \mathbf{E} = -\nabla \cdot (\mathbf{PE}) + (\mathbf{P} \cdot \nabla) \mathbf{E} \quad (91)$$

$$-(\nabla \cdot \mathbf{M}) \mathbf{H} = -\nabla \cdot (\mathbf{MH}) + (\mathbf{M} \cdot \nabla) \mathbf{H}, \quad (92)$$

and identifying $\mathbf{T}_p = -\mathbf{PE}$ and $\mathbf{g}_p = 0$ for polarization and $\mathbf{T}_m = -\mu_0 \mathbf{MH}$ and $\mathbf{g}_m = 0$ for magnetization leads to a kinetic force density

$$\mathbf{f}_{EL} = -(\mathbf{f}_e + \mathbf{f}_p + \mathbf{f}_m), \quad (93)$$

which gives

$$\boxed{\begin{aligned} \mathbf{f}_{EL} &= \frac{\partial \mathbf{P}}{\partial t} \times \mu_0 \mathbf{H} - \frac{\partial \mu_0 \mathbf{M}}{\partial t} \times \epsilon_0 \mathbf{E} \\ &\quad + \rho \mathbf{E} - \mu_0 \mathbf{H} \times \mathbf{J} + (\mathbf{P} \cdot \nabla) \mathbf{E} + \mu_0 (\mathbf{M} \cdot \nabla) \mathbf{H}. \end{aligned}} \quad (94)$$

The force density in (94) is due to Einstein and Laub [1], and has been used by others [6, 13, 16–18, 57, 59], and the relativistic form has been derived [6]. This representation has also been called the Chu Formulation [6]. The three coupled systems in (94), each with a stress tensor, result in a net stress tensor given by $\mathbf{T}_e + \mathbf{T}_p + \mathbf{T}_m = \mathbf{T}$ which is given by

$$\mathbf{T}_{EL} = \frac{1}{2} (\epsilon_0 E^2 + \mu_0 H^2) \mathbf{I} - \mathbf{D}\mathbf{E} - \mathbf{B}\mathbf{H}. \quad (95)$$

Note that \mathbf{T}_{EL} is not necessarily symmetric. Notice also that material dispersion can be incorporated through the time derivatives of \mathbf{P} and \mathbf{M} in (87) and (94). For plane waves in locally homogeneous isotropic media and referring to (87), $\nabla \cdot \mathbf{E} = 0$ and $\nabla \cdot \mathbf{H} = 0$. However, for general material arrangements and beam profiles, $(\mathbf{P} \cdot \nabla)\mathbf{E}$ and $(\mathbf{M} \cdot \nabla)\mathbf{H}$ in (94) can be nonzero. In the case of a normally incident plane wave on a surface,

$$\mathbf{f}_{NPW} = \frac{\partial \mathbf{P}}{\partial t} \times \mu_0 \mathbf{H} - \frac{\partial \mu_0 \mathbf{M}}{\partial t} \times \epsilon_0 \mathbf{E} - \mu_0 \mathbf{H} \times \mathbf{J}, \quad (96)$$

with SI units of Nm^{-3} and where the subscript on \mathbf{f} indicates that this expression holds for a normally incident plane wave.

4.3 Initial Analysis of Einstein-Laub Formulation

An important point related to the credibility of (94) is the static limit in magnetic materials, and consistency with the work of Lorentz (36). In fact, a major concern has been that there appears to be an inconsistency to explain. We address this issue now. Later we will consider the explanation of optical force experiments.

The immediate challenge is that (94) has $\mathbf{J} \times \mu_0 \mathbf{H}$, while for the static case we indicated experiments (and Lorentz microscopy) suggest that it should be $\mathbf{J} \times \mathbf{B}$. It has earlier been proposed that the root of the issue is that (94) applies to local, homogenized media, and the situation of charges passing through media is more complicated and may not conform [6]. However, \mathbf{J} is an impressed current (a mathematical source) that can encompass Ohm's law and the steady current when $\partial \mathbf{P} / \partial t \rightarrow 0$, or is an equivalent current (in the Huygen's sense). Introducing an electron beam into a sample, where we make the assumption of uniform velocity, would appear to be captured in \mathbf{J} . Superficially, there appears to be an issue with consistency between (94) and (36).

All material characteristics (including dispersion and free and bound charge) are captured by \mathbf{P} and \mathbf{M} in (94). This equation was developed assuming that all material characteristics are captured in the various charges and their motion, and that the fields are \mathbf{E} and \mathbf{H} . Other forms are possible and one might wonder if another form may be needed?

We use the identity $(\nabla \mathbf{b}) \cdot \mathbf{a} = (\mathbf{a} \cdot \nabla) \mathbf{b} + \mathbf{a} \times (\nabla \times \mathbf{b})$, with tensor operation $(\nabla \mathbf{b})_{ij} = \partial b_j / \partial x_i$ [6], to write

$$(\nabla \mathbf{H}) \cdot \mathbf{M} = (\mathbf{M} \cdot \nabla) \mathbf{H} + \mathbf{M} \times (\nabla \times \mathbf{H}). \quad (97)$$

Therefore, referring to (94),

$$\begin{aligned} \mu_0 (\mathbf{M} \cdot \nabla) \mathbf{H} &= \mu_0 (\nabla \mathbf{H}) \cdot \mathbf{M} - \mu_0 \mathbf{M} \times (\nabla \times \mathbf{H}) \\ &= \mu_0 (\nabla \mathbf{H}) \cdot \mathbf{M} + \mathbf{J} \times \mu_0 \mathbf{M}, \end{aligned} \quad (98)$$

where we have used Ampere's law for magnetostatics, hence ignoring displacement current (to investigate the relation between (94) for the **static case** and the Lorentz result). Using (98), and

considering the two relevant terms in (94), we have

$$\begin{aligned}
\mathbf{J} \times \mu_0 \mathbf{H} + \mu_0 (\mathbf{M} \cdot \nabla) \mathbf{H} &= \mathbf{J} \times \mu_0 \mathbf{H} + \mu_0 (\nabla \mathbf{H}) \cdot \mathbf{M} + \mathbf{J} \times \mu_0 \mathbf{M} \\
&= \mathbf{J} \times \mathbf{B} + \mu_0 (\nabla \mathbf{H}) \cdot \mathbf{M} \\
&\approx \mathbf{J} \times \mathbf{B},
\end{aligned} \tag{99}$$

where the approximation assumes that the local, mean field is approximately constant over the length scale of interest - this is a force density. This is equivalent to a mean field theory where the local mean is constant, and this is compatible with the local homogenization assumption. *Equation (99) indicates that (94) is consistent with the result from Lorentz for the static case. This key point does not seem to have been recognized previously.*

Let us consider the electrostatic situation. Using the same vector identity that led to (97),

$$\begin{aligned}
(\nabla \mathbf{E}) \cdot \mathbf{P} &= (\mathbf{P} \cdot \nabla) \mathbf{E} + \mathbf{P} \times (\nabla \times \mathbf{E}) \\
&= (\mathbf{P} \cdot \nabla) \mathbf{E},
\end{aligned} \tag{100}$$

because the electrostatic field has zero curl. Using the same locally constant field assumption, that $\nabla \mathbf{E} \approx 0$, we see that $(\mathbf{P} \cdot \nabla) \mathbf{E} \approx 0$. Hence, in the static limit, (94) becomes

$$\lim_{\omega \rightarrow 0} \mathbf{f}_{EL} = \rho \mathbf{E} + \mathbf{J} \times \mathbf{B}, \tag{101}$$

with the assumption that the local field in this small volume is independent of position. *Equation (101) suggests that the Einstein-Laub formulation is consistent with the accepted static form of the Lorentz force.*

4.4 A Different Minkowski Formulation

Another development has been attributed to a Minkowski representation that uses the Abraham form of the momentum [6, 34]. Chu, Penfield, and Haus consider relativistic forms and differences between the Chu (Einstein-Laub) form and their interpretation of that associated with Minkowski, and show that the two forms are consistent [34]. For completeness, we review this development for the static medium.

Using the Minkowski stress tensor of form

$$\mathbf{T}_M = (\mathbf{D} \cdot \mathbf{E} + \mathbf{B} \cdot \mathbf{H}) \mathbf{I} - \mathbf{D}\mathbf{E} - \mathbf{B}\mathbf{H} \tag{102}$$

and an analogous procedure as in Section 4.1, the sum of $\mathbf{D} \times (1)$ and $\mathbf{B} \times (2)$ gives

$$\mathbf{D} \times (\nabla \times \mathbf{E}) + \mathbf{B} \times (\nabla \times \mathbf{H}) = - \left(\frac{\partial \mathbf{D}}{\partial t} \times \mathbf{B} + \mathbf{D} \times \frac{\partial \mathbf{B}}{\partial t} \right) + \mathbf{B} \times \mathbf{J} \tag{103}$$

$$= \nabla \cdot \mathbf{T}_M + (\nabla \cdot \mathbf{E}) \mathbf{D} + (\nabla \cdot \mathbf{H}) \mathbf{B}. \tag{104}$$

Using the Abraham momentum (53) to form the kinetic force density using a procedure similar to

that to achieve (84) and (88) gives

$$\begin{aligned}
\mathbf{f}_{AM} &= - \left(\nabla \cdot \mathbf{T}_M + \frac{\partial \mathbf{g}_A}{\partial t} \right) \\
&= - \frac{\partial \mathbf{g}_A}{\partial t} + \left(\frac{\partial \mathbf{D}}{\partial t} \times \mathbf{B} + \mathbf{D} \times \frac{\partial \mathbf{B}}{\partial t} \right) \\
&\quad - \mathbf{B} \times \mathbf{J} + (\nabla \cdot \mathbf{E}) \mathbf{D} + (\nabla \cdot \mathbf{H}) \mathbf{D} \\
&= \mathbf{f}_{EL} + \frac{1}{c^2} \frac{\partial \mathbf{E}}{\partial t} \times \mathbf{M} + \frac{\partial \mathbf{P}}{\partial t} \times \mathbf{B} + \mathbf{P} \times \frac{\partial \mu_0 \mathbf{M}}{\partial t} - \mu_0 \mathbf{M} \times \mathbf{J} \\
&\quad (\nabla \cdot \mathbf{E}) \mathbf{D} + (\nabla \cdot \mathbf{H}) \mathbf{D} \\
&= \frac{1}{c^2} \frac{\partial}{\partial t} (\mathbf{E} \times \mathbf{M}) + \frac{\partial}{\partial t} (\mathbf{P} \times \mathbf{B}) - \mathbf{B} \times \mathbf{J} + (\nabla \cdot \mathbf{E}) \mathbf{D} + (\nabla \cdot \mathbf{H}) \mathbf{D},
\end{aligned} \tag{106}$$

where \mathbf{f}_{AM} indicates that the Abraham momentum was used with the Minkowski stress tensor. However, one might suspect that this manipulation with Maxwell's equations should yield the Einstein-Laub force (or the Chu force), as noted by Penfield and Haus [6, 34]. Using our terminology, $\mathbf{T}_{EL} + \mathbf{T}_C = \mathbf{T}_M$, where \mathbf{T}_C is an addition to the Einstein-Laub stress tensor to form Minkowski stress tensor. This yields

$$\begin{aligned}
\mathbf{f}_{AM} &= - \left[\nabla \cdot (\mathbf{T}_{EL} + \mathbf{T}_C) + \frac{\partial \mathbf{g}_A}{\partial t} \right] \\
&= \mathbf{f}_{EL} - \nabla \cdot \mathbf{T}_C.
\end{aligned} \tag{107}$$

The point made by Chu, Penfield and Haus is that, of course, a single force density expression results when the same stress tensor is used. An important point is that they describe this as the *Minkowski form*, because of the form of Maxwell's equations used, but they use the *Abraham momentum and not the Minkowski momentum*. For example, the last two terms in (106) have associated terms in \mathbf{T}_M , leading to the conclusion that this form can be simplified to that of Einstein and Laub.

4.5 Other Prospects with the Abraham Momentum

One can take the cross product of (2) with $\epsilon_0 \mathbf{E}$ and (1) with \mathbf{B} and proceed with the use of the Abraham momentum. While the vector algebra with Maxwell's equations follows consistently, another stress tensor and hence force expression results. These do not appear meaningful. Likewise, the products could be (1) by \mathbf{D} and (2) by \mathbf{B} , and one could consider use of the Minkowski stress tensor (see the next section). However, the seemingly redundant terms in this approach suggest that this is not a productive direction.

5 Force Theory with the Minkowski Momentum

It is too simplistic to consider $\mathbf{g}_M = n^2 \mathbf{g}_A$, where n is the refractive index, because this assumes the refractive index is a real quantity, which cannot be the case at an arbitrary frequency, and it does not apply to the general anisotropic material situation. We therefore interpret the Minkowski momentum as

$$\mathbf{D} \times \mathbf{B} = (\epsilon_0 \mathbf{E} + \mathbf{P}) \times \mu_0 (\mathbf{H} + \mathbf{M}). \tag{108}$$

Consider the sum of $\mathbf{D} \times (1)$ and $\mathbf{B} \times (2)$, which gives with the use of the Minkowski momentum,

$$\mathbf{D} \times (\nabla \times \mathbf{E}) + \mathbf{B} \times (\nabla \times \mathbf{H}) = - \frac{\partial \mathbf{g}_M}{\partial t} + \mathbf{B} \times \mathbf{J}. \tag{109}$$

By analogy with (78),

$$\mathbf{D} \times (\nabla \times \mathbf{E}) + \mathbf{B} \times (\nabla \times \mathbf{H}) = \nabla \cdot \mathbf{T}_M + (\nabla \cdot \mathbf{E}) \mathbf{D} + (\nabla \cdot \mathbf{H}) \mathbf{B}. \quad (110)$$

Using (110) in (109) leads to

$$\begin{aligned} \mathbf{f}_e &= \nabla \cdot \mathbf{T}_M + \frac{\partial \mathbf{g}_M}{\partial t} \\ &= -(\nabla \cdot \mathbf{E}) \mathbf{D} - (\nabla \cdot \mathbf{H}) \mathbf{B} + \mathbf{B} \times \mathbf{J}. \end{aligned} \quad (111)$$

This results in a kinetic force density

$$\begin{aligned} \mathbf{f}_k &= -\mathbf{f}_e \\ &= (\nabla \cdot \mathbf{E}) \mathbf{D} + (\nabla \cdot \mathbf{H}) \mathbf{B} - \mathbf{B} \times \mathbf{J}. \end{aligned} \quad (112)$$

Equation (112) does not have a radiation pressure (power flow) term and hence does not make physical sense. Penfield and Haus [6] have noted that there is no justification that (102) and \mathbf{g}_M used here describe the system in any meaningful way.

We consider now a modification of the Einstein-Laub development that uses the Minkowski momentum. We can write (81) as

$$\nabla \cdot \mathbf{T}_e + \epsilon_0 (\nabla \cdot \mathbf{E}) \mathbf{E} + \mu_0 (\nabla \cdot \mathbf{H}) \mathbf{H} = -\epsilon_0 \mathbf{E} \times \frac{\partial \mathbf{B}}{\partial t} + \mu_0 \mathbf{H} \times \frac{\partial \mathbf{D}}{\partial t} + \mu_0 \mathbf{H} \times \mathbf{J}, \quad (113)$$

where \mathbf{T}_e is given by (77). Using the Minkowski form of the electromagnetic momentum in (54), (113) can be written as

$$\nabla \cdot \mathbf{T}_e + \epsilon_0 (\nabla \cdot \mathbf{E}) \mathbf{E} + \mu_0 (\nabla \cdot \mathbf{H}) \mathbf{H} = -\frac{\partial \mathbf{g}_M}{\partial t} + \mathbf{P} \times \frac{\partial \mathbf{B}}{\partial t} - \mu_0 \mathbf{M} \times \frac{\partial \mathbf{D}}{\partial t} + \mu_0 \mathbf{H} \times \mathbf{J}. \quad (114)$$

Setting

$$\mathbf{f}_e = \nabla \cdot \mathbf{T}_e + \frac{\partial \mathbf{g}_M}{\partial t} \quad (115)$$

in (114), and with use of (37) and (38), gives

$$\begin{aligned} \mathbf{f}_e &= \mathbf{P} \times \frac{\partial \mathbf{B}}{\partial t} - \mu_0 \mathbf{M} \times \frac{\partial \mathbf{D}}{\partial t} + \mu_0 \mathbf{H} \times \mathbf{J} \\ &+ (\nabla \cdot \mathbf{P}) \mathbf{E} - \rho \mathbf{E} + \mu_0 (\nabla \cdot \mathbf{M}) \mathbf{H}. \end{aligned} \quad (116)$$

Following a procedure similar to that used in the development of (94),

$$\begin{aligned} \mathbf{f}_M &= -(\mathbf{f}_e + \mathbf{f}_p + \mathbf{f}_m) \\ &= -\mathbf{P} \times \frac{\partial \mathbf{B}}{\partial t} + \mu_0 \mathbf{M} \times \frac{\partial \mathbf{D}}{\partial t} \\ &+ \rho \mathbf{E} - \mu_0 \mathbf{H} \times \mathbf{J} + (\mathbf{P} \cdot \nabla) \mathbf{E} + \mu_0 (\mathbf{M} \cdot \nabla) \mathbf{H}, \end{aligned} \quad (117)$$

where \mathbf{f}_M refers to a possibly legitimate force density expression based on the use of the Minkowski momentum. Equation (117) appears to have been derived for the first time here. For non-magnetic, electric materials, (117) becomes

$$\mathbf{f}_{ME} = -\mathbf{P} \times \frac{\partial \mu_0 \mathbf{H}}{\partial t} + \rho \mathbf{E} + (\mathbf{P} \cdot \nabla) \mathbf{E} - \mu_0 \mathbf{H} \times \mathbf{J}. \quad (118)$$

Equation (118) has a radiation pressure sign (for CW radiation) opposite to (94). Our work has shown that the latter gives rise to positive pressure on a lossless dielectric slab [57], so (118) cannot be correct.

Our conclusion is that while the Minkowski momentum has physical significance, rigorous incorporation into a field-based force density appears problematic. The approaches here are unfruitful and are hence discounted as candidates.

6 Note on $(\nabla \cdot \mathbf{P}) \mathbf{E}$ and $(\mathbf{P} \cdot \nabla) \mathbf{E}$

The descriptions of force density have important differences in the terms $(\nabla \cdot \mathbf{P}) \mathbf{E}$ and $(\mathbf{P} \cdot \nabla) \mathbf{E}$ that warrant special mention here to make the point clear. We define a curvilinear coordinate system as (x_1, x_2, x_3) and

$$\nabla = \hat{x}_1 \frac{\partial}{\partial x_1} + \hat{x}_2 \frac{\partial}{\partial x_2} + \hat{x}_3 \frac{\partial}{\partial x_3}. \quad (119)$$

We then have

$$(\nabla \cdot \mathbf{P}) \mathbf{E} = \left(\frac{\partial P_1}{\partial x_1} + \frac{\partial P_2}{\partial x_2} + \frac{\partial P_3}{\partial x_3} \right) \mathbf{E} \quad (120)$$

and

$$(\mathbf{P} \cdot \nabla) \mathbf{E} = \left(P_1 \frac{\partial}{\partial x_1} + P_2 \frac{\partial}{\partial x_2} + P_3 \frac{\partial}{\partial x_3} \right) \mathbf{E}. \quad (121)$$

In the case of (locally) homogeneous and isotropic material with $\mathbf{P} = \epsilon_0 \chi_E \mathbf{E}$, in the frequency domain, (120) and (121) become

$$(\nabla \cdot \mathbf{P}) \mathbf{E} = \begin{bmatrix} E_1 \frac{\partial P_1}{\partial x_1} + E_1 \frac{\partial P_2}{\partial x_2} + E_1 \frac{\partial P_3}{\partial x_3} \\ E_2 \frac{\partial P_1}{\partial x_1} + E_2 \frac{\partial P_2}{\partial x_2} + E_2 \frac{\partial P_3}{\partial x_3} \\ E_3 \frac{\partial P_1}{\partial x_1} + E_3 \frac{\partial P_2}{\partial x_2} + E_3 \frac{\partial P_3}{\partial x_3} \end{bmatrix} \quad (122)$$

$$= \epsilon_0 \chi_E \begin{bmatrix} E_1 \frac{\partial E_1}{\partial x_1} + E_1 \frac{\partial E_2}{\partial x_2} + E_1 \frac{\partial E_3}{\partial x_3} \\ E_2 \frac{\partial E_1}{\partial x_1} + E_2 \frac{\partial E_2}{\partial x_2} + E_2 \frac{\partial E_3}{\partial x_3} \\ E_3 \frac{\partial E_1}{\partial x_1} + E_3 \frac{\partial E_2}{\partial x_2} + E_3 \frac{\partial E_3}{\partial x_3} \end{bmatrix}. \quad (123)$$

$$(\mathbf{P} \cdot \nabla) \mathbf{E} = \begin{bmatrix} P_1 \frac{\partial E_1}{\partial x_1} + P_2 \frac{\partial E_1}{\partial x_2} + P_3 \frac{\partial E_1}{\partial x_3} \\ P_1 \frac{\partial E_2}{\partial x_1} + P_2 \frac{\partial E_2}{\partial x_2} + P_3 \frac{\partial E_2}{\partial x_3} \\ P_1 \frac{\partial E_3}{\partial x_1} + P_2 \frac{\partial E_3}{\partial x_2} + P_3 \frac{\partial E_3}{\partial x_3} \end{bmatrix} \quad (124)$$

$$= \epsilon_0 \chi_E \begin{bmatrix} E_1 \frac{\partial E_1}{\partial x_1} + E_2 \frac{\partial E_1}{\partial x_2} + E_3 \frac{\partial E_1}{\partial x_3} \\ E_1 \frac{\partial E_2}{\partial x_1} + E_2 \frac{\partial E_2}{\partial x_2} + E_3 \frac{\partial E_2}{\partial x_3} \\ E_1 \frac{\partial E_3}{\partial x_1} + E_2 \frac{\partial E_3}{\partial x_2} + E_3 \frac{\partial E_3}{\partial x_3} \end{bmatrix} \quad (125)$$

Note the important differences in the vector components of these expressions.

We also note that the fields in any locally homogeneous material domain can be exactly decomposed into a superposition of plane waves, i.e., into a spatial Fourier representation. A plane wave is divergenceless, and linearity in the superposition means that any field represented by a plane wave superposition is divergenceless. Hence any field in a locally homogeneous (and source-free) region is divergenceless. This means that $\nabla \cdot \mathbf{P} = 0$ in a homogeneous region. However, there will be discontinuities associated with surface charge densities at interfaces, meaning that this term could contribute to the force at an interface.

7 Lorentz Forces from Stress tensor

7.1 Lorentz Electrostatic Force

Consider now a check based on the static Lorentz force. From (77), the stress tensor for electrostatics becomes

$$\mathbf{T}_e = \frac{1}{2}\epsilon_0 E^2 \mathbf{I} - \epsilon_0 \mathbf{E}\mathbf{E}, \quad (126)$$

and from (78)

$$\nabla \cdot \mathbf{T}_e = -\epsilon_0 (\nabla \cdot \mathbf{E}) \mathbf{E}. \quad (127)$$

The electrostatic part of the Lorentz force density from (36) is

$$\begin{aligned} \rho \mathbf{E} &= (\nabla \cdot \mathbf{D}) \mathbf{E} \\ &= \epsilon_0 (\nabla \cdot \mathbf{E}) \mathbf{E} + (\nabla \cdot \mathbf{P}) \mathbf{E}. \end{aligned} \quad (128)$$

Using the identity $\nabla \cdot (\mathbf{a}\mathbf{b}) = (\nabla \cdot \mathbf{a})\mathbf{b} + (\mathbf{a} \cdot \nabla)\mathbf{b}$ [6] and substituting (127) in (128) gives

$$\mathbf{f} = -\nabla \cdot \mathbf{T}_e - \nabla \cdot \mathbf{T}_p - (\mathbf{P} \cdot \nabla) \mathbf{E}, \quad (129)$$

where $\mathbf{T}_p = -\mathbf{P}\mathbf{E}$ as before is the polarization stress tensor. Rearranging, the kinetic force density is

$$\begin{aligned} \mathbf{f}_k &= -\nabla \cdot \mathbf{T}_e - \nabla \cdot \mathbf{T}_p \\ &= \rho \mathbf{E} + (\mathbf{P} \cdot \nabla) \mathbf{E}. \end{aligned} \quad (130)$$

With confidence, we note that (130) is the same as (41) and (94) for the static electric field cases.

7.2 Lorentz Magnetostatic Force

In analogy with the electrostatic force term from Lorentz, we consider the magnetostatic case for affirmation. From (77), the stress tensor for magnetostatics becomes

$$\mathbf{T}_h = \frac{1}{2}\mu_0 H^2 \mathbf{I} - \mu_0 \mathbf{H}\mathbf{H}, \quad (131)$$

and from (78)

$$\nabla \cdot \mathbf{T}_h = \mu_0 \mathbf{H} \times (\nabla \times \mathbf{H}) - \mu_0 (\nabla \cdot \mathbf{H}) \mathbf{H}. \quad (132)$$

Note that the left hand side of (128) is the force on a free charge density in free space. Using the dual interpretation, the magnetostatic part of the Lorentz force density in free space is

$$\mu_0 \mathbf{J} \times \mathbf{H} = \mu_0 (\nabla \times \mathbf{H}) \times \mathbf{H}. \quad (133)$$

Substituting (132) in (133) gives

$$\mu_0 \mathbf{J} \times \mathbf{H} = -\nabla \cdot \mathbf{T}_h - \mu_0 (\nabla \cdot \mathbf{H}) \mathbf{H}. \quad (134)$$

Using (75), we have

$$\mu_0 \mathbf{J} \times \mathbf{H} = -\nabla \cdot \mathbf{T}_h + \mu_0 (\nabla \cdot \mathbf{M}) \mathbf{H}. \quad (135)$$

Substituting $\mu_0(\nabla \cdot \mathbf{M})\mathbf{H} = -\nabla \cdot \mathbf{T}_m - \mu_0(\mathbf{M} \cdot \nabla)\mathbf{H}$, where $\mathbf{T}_m = -\mu_0\mathbf{M}\mathbf{H}$ as before, gives

$$\mu_0\mathbf{J} \times \mathbf{H} = -\nabla \cdot \mathbf{T}_h - \nabla \cdot \mathbf{T}_m - \mu_0(\mathbf{M} \cdot \nabla)\mathbf{H}. \quad (136)$$

Rearranging, we have the kinetic force density

$$\begin{aligned} \mathbf{f}_k &= -\nabla \cdot \mathbf{T}_h - \nabla \cdot \mathbf{T}_m \\ &= \mu_0\mathbf{J} \times \mathbf{H} + \mu_0(\mathbf{M} \cdot \nabla)\mathbf{H}. \end{aligned} \quad (137)$$

Equation (137) is the magnetostatic form of (94). Under the assumption that the local field is constant, $(\nabla\mathbf{H}) \cdot \mathbf{M} \approx 0$ (see (99) and the related vector math), (137) becomes

$$\begin{aligned} \mathbf{f}_k &= \mu_0\mathbf{J} \times \mathbf{H} + \mu_0(\mathbf{M} \cdot \nabla)\mathbf{H} \\ &= \mathbf{J} \times \mu_0\mathbf{H} + \mu_0(\nabla\mathbf{H}) \cdot \mathbf{M} + \mathbf{J} \times \mu_0\mathbf{M} \\ &= \mathbf{J} \times \mathbf{B} + \mu_0(\nabla\mathbf{H}) \cdot \mathbf{M} \\ &\approx \mathbf{J} \times \mathbf{B}, \end{aligned} \quad (138)$$

The magnetostatic force development from the stress tensors therefore yields the Lorentz force in magnetized media (35).

8 Time-Averaged Force

Consider the case of modulated light. Macroscopic motion is described by the time-averaged force, given by the instantaneous force density integrated over the carrier period as

$$\langle \mathbf{f}(\mathbf{r}, t) \rangle = \frac{2\pi}{\omega_0} \int dt \mathbf{f}(\mathbf{r}, t), \quad (139)$$

where ω_0 is the circular carrier frequency. With modulated light, this averaging over carrier period produces $\langle \mathbf{f} \rangle(\mathbf{r}, t)$, with time variation dictated by the envelope $\langle \mathbf{f} \rangle(t)$.

In the case of time harmonic, monochromatic waves, and with a phasor description for the fields, the averaging produces a simple and convenient description of the force. We consider a time-harmonic, monochromatic field with frequency dependence $\exp(-i\omega t)$ and an isotropic dielectric response, giving $\mathbf{P}(\mathbf{r}, \omega) = \epsilon_0\chi_E(\mathbf{r}, \omega)\mathbf{E}(\mathbf{r}, \omega)$, with χ_E the electric susceptibility (and dielectric constant $\epsilon = 1 + \chi_E$). Likewise, the magnetization is defined as $\mathbf{M}(\mathbf{r}, \omega) = \chi_H(\mathbf{r}, \omega)\mathbf{H}(\mathbf{r}, \omega)$, with χ_H the magnetic susceptibility (and relative permeability $\mu = 1 + \chi_H$). With the frequency domain implied, the polarization can then be written as

$$\mathbf{P}(\mathbf{r}, t) = \hat{\mathbf{e}}\epsilon_0\Re\{\chi_E(\mathbf{r})E(\mathbf{r})e^{-i\omega t}\}, \quad (140)$$

where $\hat{\mathbf{e}}$ is a unit vector direction, $\Re\{\cdot\}$ is the real part, and E is the phasor electric field. By defining \mathbf{E} and \mathbf{H} similarly, the time average of the force density in (94) becomes

$$\begin{aligned} \langle \mathbf{f}_{EL} \rangle &= (\hat{\mathbf{e}} \times \hat{\mathbf{h}}) \frac{\mu_0\epsilon_0\omega}{2} \Im\{\chi_E E(\mathbf{r})H^*(\mathbf{r})\} \\ &\quad + (\hat{\mathbf{e}} \times \hat{\mathbf{h}}) \frac{\mu_0\epsilon_0\omega}{2} \Im\{E^*(\mathbf{r})\chi_H H(\mathbf{r})\} \\ &\quad + \hat{\mathbf{e}} \frac{1}{2} \Re\{\rho E^*(\mathbf{r})\} - \frac{\mu_0}{2} \Re\{\mathbf{H} \times \mathbf{J}^*\} \\ &\quad + \frac{\epsilon_0}{2} \Re\{(\chi_E E(\mathbf{r}) \hat{\mathbf{e}} \cdot \nabla)(\hat{\mathbf{e}} E^*(\mathbf{r}))\} \\ &\quad + \frac{\mu_0}{2} \Re\{(\chi_H H(\mathbf{r}) \hat{\mathbf{h}} \cdot \nabla)(\hat{\mathbf{h}} H^*(\mathbf{r}))\}, \end{aligned} \quad (141)$$

where $\Im\{\cdot\}$ is the imaginary part.

9 Force from the Stress Tensor - Stress Tensor Method

There are two possibly legitimate forms of stress tensor at this point, (95) and (102). It is common to calculate the force based on the stress tensor - which amounts to forming the divergence of the tensor with fields determined for a particular situation, and then forming the averaged force for the monochromatic case as

$$\langle \mathbf{f} \rangle = -\langle \nabla \cdot \mathbf{T} \rangle - \left\langle \frac{\partial \mathbf{g}}{\partial t} \right\rangle, \quad (142)$$

where the bra and ket represent average over the period, under the assumption that

$$\left\langle \frac{\partial \mathbf{g}}{\partial t} \right\rangle = 0. \quad (143)$$

Consider the time-averaged electromagnetic force due to monochromatic light, with $\mathbf{E}(t) = \hat{\mathbf{e}} \Re\{E \exp(-i\omega t)\}$ and $\mathbf{H}(t) = \hat{\mathbf{h}} \Re\{H \exp(-i\omega t)\}$ and $\hat{\mathbf{e}} \times \hat{\mathbf{h}} = \hat{\mathbf{s}}$. For the Abraham momentum, and using $E = E' + iE''$ and $H = H' + iH''$, we have

$$\begin{aligned} \frac{\partial}{\partial t}(\mathbf{E} \times \mathbf{H}) &= \hat{\mathbf{s}} \frac{\partial}{\partial t} (\Re\{E e^{-i\omega t}\} \Re\{H e^{-i\omega t}\}) \\ &= \hat{\mathbf{s}} [\Re\{-i\omega(E' + iE'')(\cos \omega t - i \sin \omega t)\} \Re\{(H' + iH'')(\cos \omega t - i \sin \omega t)\} \\ &\quad + \Re\{(E' + iE'')(\cos \omega t - i \sin \omega t)\} \Re\{-i\omega(H' + iH'')(\cos \omega t - i \sin \omega t)\}] \\ &= \hat{\mathbf{s}} [(-\omega E' \sin \omega t + \omega E'' \cos \omega t)(H' \cos \omega t + H'' \sin \omega t) \\ &\quad (E' \cos \omega t + \omega E'' \sin \omega t)(-\omega H' \sin \omega t + \omega H'' \cos \omega t)]. \end{aligned} \quad (144)$$

Therefore, the time average becomes

$$\begin{aligned} \left\langle \frac{\partial}{\partial t}(\mathbf{E} \times \mathbf{H}) \right\rangle &= \hat{\mathbf{s}} [-\omega E' H'' \langle \sin^2 \omega t \rangle + \omega E'' H' \langle \cos^2 \omega t \rangle + \omega E' H'' \langle \cos^2 \omega t \rangle - \omega E'' H' \langle \sin^2 \omega t \rangle] \\ &= 0. \end{aligned} \quad (145)$$

Using similar math for the Minkowski case,

$$\left\langle \frac{\partial}{\partial t}(\mathbf{D} \times \mathbf{B}) \right\rangle = 0, \quad (146)$$

even for anisotropic materials, where the cross product could have three orthogonal unit vector components. Based upon the correct \mathbf{T} in (142), the force density for monochromatic waves in physical media can be found from

$$\langle \mathbf{f} \rangle = -\langle \nabla \cdot \mathbf{T} \rangle. \quad (147)$$

However, the general, non-local in time constitutive relations (specified in the frequency domain) need to be used. There is also, of course, the question of what stress tensor is correct.

Now we develop this picture for *modulated waves* and for simple, isotropic constitutive parameters. We draw on our earlier work [60] with a change of variables. We write

$$\left\langle \frac{\partial}{\partial t}(\mathbf{E} \times \mathbf{H}) \right\rangle = \left\langle \frac{\partial \mathbf{E}}{\partial t} \times \mathbf{H} \right\rangle + \left\langle \mathbf{E} \times \frac{\partial \mathbf{H}}{\partial t} \right\rangle. \quad (148)$$

Enforcing reality, we write the inverse Fourier transform of the fields as

$$\mathbf{E}(t) = \frac{1}{4\pi} \int \mathbf{E}(\omega) e^{-i\omega t} d\omega + c.c. \quad (149)$$

$$\mathbf{H}(t) = \frac{1}{4\pi} \int \mathbf{H}(\omega) e^{-i\omega t} d\omega + c.c., \quad (150)$$

which could also be written with different coefficients, depending on how the Fourier transform is defined. This form is convenient when forming expressions in terms of a modulation envelope.

We consider now the modulated field case

$$\mathbf{E}(t) = \hat{\mathbf{e}} E(t) = \hat{\mathbf{e}} e(t) \cos(\omega_0 t) \quad (151)$$

$$\mathbf{H}(t) = \hat{\mathbf{h}} H(t) = \frac{\hat{h}}{4\pi} \int u(\omega) E(\omega) e^{-i\omega t} d\omega + c.c., \quad (152)$$

$$\mathbf{g}_A = \hat{\mathbf{e}} \times \hat{\mathbf{h}} g_A, \quad g_A = H \frac{\partial E}{\partial t} + E \frac{\partial H}{\partial t}, \quad (153)$$

where $e(t)$ is a modulation signal and $u = \eta^{-1} = (\eta_0 \sqrt{\mu/\epsilon})^{-1}$, with η_0 the free space wave impedance. The scalar form of \mathbf{g}_A in (153) is used hence forth to describe the instantaneous and the time-averaged temporal derivative of the momentum, $\langle \cdot \rangle$, the average value over the carrier period $t_0 = 2\pi/\omega_0$.

Assuming a slowly varying $e(t)$ (small bandwidth) in (151) [61],

$$\frac{\partial E}{\partial t} \approx -\omega_0 e(t) \sin(\omega_0 t) + \frac{\partial e(t)}{\partial t} \cos(\omega_0 t). \quad (154)$$

With a Taylor series expansion of $u(\omega)$, from (152),

$$\begin{aligned} H &\approx e(t) [u'(\omega_0) \cos(\omega_0 t) + u''(\omega_0) \sin(\omega_0 t)] \\ &+ \frac{\partial e(t)}{\partial t} \left[\frac{\partial u'}{\partial \omega} \Big|_{\omega_0} \sin(\omega_0 t) - \frac{\partial u''}{\partial \omega} \Big|_{\omega_0} \cos(\omega_0 t) \right]. \end{aligned} \quad (155)$$

Using (154) and (155),

$$\left\langle H \frac{\partial E}{\partial t} \right\rangle \approx C_1 e^2(t) + C_2 e(t) \frac{\partial e(t)}{\partial t} + C_3 \left[\frac{\partial e(t)}{\partial t} \right]^2, \quad (156)$$

with

$$\begin{aligned} C_1 &\equiv -\frac{\omega_0}{2} u''(\omega_0) \\ C_2 &\equiv \frac{1}{2} \frac{\partial(\omega u')}{\partial \omega} \Big|_{\omega_0} \\ C_3 &\equiv -\frac{1}{2} \frac{\partial u''}{\partial \omega} \Big|_{\omega_0}. \end{aligned} \quad (157)$$

Noting that $H(t)$ is of the form of $E(t)$ with $E(\omega) \rightarrow uE(\omega)$, and following a similar procedure as that used to obtain (154) [61], we find

$$\begin{aligned} \frac{\partial H}{\partial t} &\approx \omega_0 e(t) [u''(\omega_0) \cos(\omega_0 t) - u'(\omega_0) \sin(\omega_0 t)] + \frac{\partial e(t)}{\partial t} \left[\frac{\partial(\omega u')}{\partial \omega} \Big|_{\omega=\omega_0} \cos(\omega_0 t) \right. \\ &\left. + \frac{\partial(\omega u'')}{\partial \omega} \Big|_{\omega=\omega_0} \sin(\omega_0 t) \right]. \end{aligned} \quad (158)$$

Using (151) and (158), we obtain

$$\left\langle E \frac{\partial H}{\partial t} \right\rangle \approx e^2(t)D_1 + e(t)\frac{\partial e(t)}{\partial t}D_2, \quad (159)$$

with

$$\begin{aligned} D_1 &\equiv \frac{\omega_0}{2}u''(\omega_0) \\ D_2 &\equiv \frac{1}{2}\frac{\partial(\omega u')}{\partial\omega}\Big|_{\omega_0} \end{aligned} \quad (160)$$

Note that the form of (156) and (159) differ because we use the electric field as the basis. From (156) and (159),

$$\begin{aligned} \left\langle \frac{\partial g_A}{\partial t} \right\rangle &= (C_1 + D_1)e^2(t) + (C_2 + D_2)e(t)\frac{\partial e(t)}{\partial t} + C_3 \left[\frac{\partial e(t)}{\partial t} \right]^2 \\ &= \frac{\partial(\omega u')}{\partial\omega}\Big|_{\omega_0} e(t)\frac{\partial e(t)}{\partial t} + \frac{1}{2}\frac{\partial u''}{\partial\omega}\Big|_{\omega_0} \left[\frac{\partial e(t)}{\partial t} \right]^2. \end{aligned} \quad (161)$$

Note that $C_1 + D_1 = 0$ is consistent with the monochromatic case. However, the presence of the terms related to the derivative of the field envelope in (161) indicate that these terms are non-zero with modulated radiation. In this case, the divergence of the stress tensor does not give the force density.

10 Torque

In addition to linear momentum, electromagnetic waves carry angular momentum, a spin part associated with polarization and an orbital part related to spatial distribution [62–64]. Laguerre-Gaussian (or Hermite-Gaussian) modes have well defined orbital angular momentum, leading to a proposed experiment to measure torque [62] and measurement results (see [65]). The topic of torque theory requires more work. At this point we make several observations.

One might anticipate that with the linear force density (\mathbf{f}) we can form the torque density as

$$\mathbf{t} = \mathbf{r} \times \mathbf{f}, \quad (162)$$

for some radial arm \mathbf{r} from a reference point about which the torque is determined. In fact this has been used in relation to experiments [66], has been used as a Lorentz torque density [44], and is consistent with field angular momentum math [62]. However, torque density theory has received little attention (see comments along these lines and recent contributions [65, 67]). In one experiment [68], it was found that the torque density was given by

$$\mathbf{t}_E = \mathbf{P} \times \mathbf{E}. \quad (163)$$

The magnetic counterpart is

$$\mathbf{t}_M = \mathbf{M} \times \mathbf{H}. \quad (164)$$

Evaluation of (162) and the contributions of (163) and (164) are needed.

11 Description of Experiments

11.1 Prediction of the Jones and Leslie Experiments

We explained the 1978 experiments by Jones and Leslie, showing that the radiation pressure on a mirror depends on the background medium refractive index, using a force model [69]. Those experimental results were predicted for the first time using a force representation that incorporates the Abraham momentum by utilizing the power calibration method employed in the Jones and Leslie experiments. Extending the same procedure, the polarization and angle independence of the experimental data was also explained by this model. Prospects are good for this general form of the electromagnetic force density to be effective in predicting other experiments with macroscopic materials. Furthermore, the rigorous representation of material dispersion makes the representation important for metamaterials that operate in the vicinity of homogenized material resonances.

A single plane wave representation is considered with illumination of a perfect mirror at angle θ_i in a background (liquid) medium of refractive index $n = \sqrt{\epsilon_l}$, with ϵ_l the dielectric constant, as in the Jones and Leslie experiments [22]. The laser coherence is assumed to be sufficiently high so as to allow a monochromatic picture. Consider then time harmonic fields and the incident wave vector as $\mathbf{k} = k_x \hat{x} + k_z \hat{z} = k_l \hat{k}$, so $\cos \theta_i = k_z/k_l$. The multilayer dielectric stack mirror used by Jones and Leslie is modeled as a perfect electric conductor (PEC). Doing so assumes that the light is totally reflected and the specific structure of the fields near to the surface of this one-dimensional photonic crystal can be neglected. In another view, the problem is treated by a Huygen's equivalent electric current source existing on the $z = 0$ surface. From (96), this results in a time-averaged force density directly applied to the mirror of

$$\langle \mathbf{f}_j \rangle = -\frac{\mu_0}{2} \Re(\mathbf{H} \times \mathbf{J}^*), \quad (165)$$

where \Re is the real part, and \mathbf{H} and \mathbf{J} are phasor frequency domain quantities that are distinguished from the temporal form by context. The mirror surface is assumed to have global coordinates such that the normal into the incident field space is $-\hat{z}$ and the mirror surface is at $z = 0$. From the boundary condition on the tangential magnetic field applied in (165), the pressure on the mirror (Nm^{-2}) is

$$\begin{aligned} \langle \mathbf{F}_j \rangle &= -\frac{\mu_0}{2} \Re(\mathbf{H}_{z=0} \times \mathbf{J}_s^*) \\ &= \frac{\mu_0}{2} \Re[\mathbf{H}_{z=0} \times (\hat{z} \times \mathbf{H}_{z=0}^*)], \end{aligned} \quad (166)$$

where \mathbf{J}_s A/m is the surface electric current density.

For a TE plane wave (E_y, H_x, H_z) in the temporal frequency domain,

$$\mathbf{E} = \hat{y} E_0 e^{ik_x x} \left(e^{ik_z z} + \Gamma_e e^{-ik_z z} \right) \quad (167)$$

$$\mathbf{H} = -\hat{x} \frac{E_0}{Z_z} e^{ik_x x} \left(e^{ik_z z} - \Gamma_e e^{-ik_z z} \right) + \hat{z} \frac{E_0}{Z_x} e^{ik_x x} \left(e^{ik_z z} + \Gamma_e e^{-ik_z z} \right), \quad (168)$$

with $\Gamma_e = -1$ for a PEC mirror and TE impedances $Z_z = \omega \mu_0 / k_z$ and $Z_x = \omega \mu_0 / k_x$. For TM polarization (H_y, E_x, E_z),

$$\mathbf{H} = \hat{y} H_0 e^{ik_x x} \left(e^{ik_z z} + \Gamma_h e^{-ik_z z} \right) \quad (169)$$

$$\mathbf{E} = \hat{x} H_0 Z_z e^{ik_x x} \left(e^{ik_z z} - \Gamma_h e^{-ik_z z} \right) - \hat{z} H_0 Z_x e^{ik_x x} \left(e^{ik_z z} + \Gamma_h e^{-ik_z z} \right), \quad (170)$$

with $\Gamma_h = 1$ for a PEC mirror and TM impedances $Z_z = k_z/(\omega\epsilon_0\epsilon)$ and $Z_x = k_x/(\omega\epsilon_0\epsilon)$. Considering monochromatic waves, the time domain fields corresponding to (167) - (170) are defined by $\mathbf{E}(x, z, t) = \Re[\mathbf{E}(x, z, \omega) \exp(-i\omega t)]$, with ω the Fourier conjugate variable associated with t and for the electric field.

For the TE case, substituting (168) with $\Gamma_e = -1$ and $z = 0$ into (166) gives

$$\begin{aligned}\langle \mathbf{F}_j \rangle_{TE} &= \hat{z} 2\mu_0 \frac{|E_0|^2}{|Z_z|^2} \\ &= \hat{z} 2\mu_0 |E_0|^2 \frac{\cos^2 \theta_i}{|\eta_l|^2},\end{aligned}\tag{171}$$

where η_l is the wave impedance of the liquid. From (169) and (166), the TM pressure is

$$\begin{aligned}\langle \mathbf{F}_j \rangle_{TM} &= \hat{z} 2\mu_0 |H_0|^2 \\ &= \hat{z} 2\mu_0 \frac{|E_0|^2}{|\eta_l|^2}.\end{aligned}\tag{172}$$

Note that the forces in (171) and (172) depend on the impedance of the background, so changing the sign of the refractive index does not change the sign of the force.

The exact time-averaged force density in the liquid in which the mirror is inserted, from (96) and for monochromatic light, is [17]

$$\begin{aligned}\langle \mathbf{f}_d \rangle &= \left\langle \frac{\partial \mathbf{P}}{\partial t} \times \mu_0 \mathbf{H} \right\rangle \\ &= \frac{\omega \mu_0 \epsilon_0}{2} \Im(\chi_E \mathbf{E} \times \mathbf{H}^*),\end{aligned}\tag{173}$$

where \Im is the imaginary part, and we have set $\mathbf{P} = \epsilon_0 \chi_E \mathbf{E}$, with $\chi_E = \epsilon_l - 1$ the assumed isotropic electric susceptibility. There are two contributors to $\langle \mathbf{f}_d \rangle$, that due to χ_E'' , where $\chi_E = \chi_E' + i\chi_E''$, and that associated with the standing wave within the beam region where the incident and reflected fields overlap in the neighborhood of the mirror. Any force imparted to the liquid could produce a mechanical force on the mirror. However, the liquids used in the experiments had small loss [22], so the force on the mirror due to absorption in the background liquid is neglected and the dielectric constant of the background is assumed to be real. The \hat{z} -component of the force density near the mirror for the TE case, from (173) for a lossless liquid, is

$$\begin{aligned}\langle \mathbf{f}_d \rangle &= -\hat{z} \frac{\omega \mu_0 \epsilon_0}{2} \Im(\chi_E' E_y H_x^*) \\ &= \hat{z} \epsilon_0 (\epsilon_l' - 1) |E_0|^2 k_z \sin(2k_z z),\end{aligned}\tag{174}$$

where $\epsilon_l' = \Re(\epsilon_l)$ and $k_z = \sqrt{k_l^2 - k_x^2}$ has been assumed real. The total z -dependent pressure on the liquid becomes

$$\langle \mathbf{F}_d \rangle = \int_{z \rightarrow -\infty}^0 \langle \mathbf{f}_d \rangle dz.\tag{175}$$

In the Jones and Leslie experiment [22], the compact beam (with a 0.6 mm spot) is incident on the mirror at 6.4° , meaning that there is a standing wave pattern with triangular support that reduces as one moves away from the mirror (in the $-z$ -direction, referring to (174)). Consequently, there is a small net negative pressure for each period of the standing wave at the extremities. Small loss

may also enhance the standing wave near the mirror. The resulting net negative force on the liquid ($\langle \mathbf{F}_d \rangle < 0$) is related to the picture of the momentum delivered to the mirror and described by (94). The key aspect here is that this suggests there is no net pressure from the liquid applying a force to the mirror in the Jones and Leslie experiment, leading to the position that $\langle \mathbf{f}_d \rangle$ can be neglected in the determination of the force on the mirror.

It would thus appear that the pressure $\langle \mathbf{F}_j \rangle$ N/m² on a PEC mirror should explain the Jones and Leslie experiments [22]. However, the ability to do so is by no means obvious by looking at the relevant equations, (171) and (172). Jones and Leslie [22] find that the force is proportional to the background refractive index in a set of TE experiments with background liquids having various refractive indices and $\theta_i = 6.4^\circ$, unclear from either equation, and that the force is independent of polarization, certainly not evident from these equations.

The laser power was fixed by a correction method [22]. This was the major component of the calibration and accounted for reflections at the glass window, liquid interface - the reflection from which varied due the various liquids in which the mirror was immersed. The free space to glass window interface had an antireflection coating, presumably for either normal incidence or TE polarization at $\theta_i = 6.4^\circ$, and the initial set of experiments were done with TE polarization. In the single plane wave picture, this calibration corresponds to fixing the Poynting vector magnitude

$$S = \Re \left[\frac{|E_0|^2}{2\eta_l} \right] = \frac{|E_0|^2}{2\eta_0} \sqrt{\epsilon_l}, \quad (176)$$

leading to

$$|E_0|^2 = \frac{2\eta_0 S}{\sqrt{\epsilon_l}}. \quad (177)$$

Substituting (177) into (171) and (172) gives

$$\langle \mathbf{F}_j \rangle_{TE} = \hat{z} \frac{4S}{c} \cos^2 \theta_i \sqrt{\epsilon_l} \quad (178)$$

and

$$\langle \mathbf{F}_j \rangle_{TM} = \hat{z} \frac{4S}{c} \sqrt{\epsilon_l}. \quad (179)$$

Equations (178) and (179) fulfill the first requirement of predicting that the radiation pressure on the mirror is proportional to the refractive index of the background medium, $n = \sqrt{\epsilon_l}$, provided that the Poynting vector is constant. Hence, the most important conclusion here is that the Jones and Leslie experiment showing the radiation pressure is proportional to the background refractive index can be predicted with a force formulation stemming from Maxwell's equations with use of the Abraham momentum. With a \hat{z} -directed detector aperture, (178) and (179) hold with $S \rightarrow S_z$, where the quantity preserved is S_z , the z -component of the Poynting vector.

The Jones and Leslie experiments [22] show the rather surprising result that the radiation pressure is independent of polarization. The data show the ratio of the observed pressure for the two linear polarizations (TE and TM) with $\theta_i = 6.4^\circ$ for various background liquids, and for $\theta_i = 20^\circ$ for one case. The results indicate to two significant figures that the pressure is independent of polarization for $\theta_i \neq 0$. In the simplified example geometry, consider that \hat{z} is the unit vector normal to the detector. In comparing the pressure due to TE and TM, the correction factors differ because of the polarization-dependent loss, notably from the antireflection coating. Therefore, the argument here is that S_z is maintained constant in the power calibration.

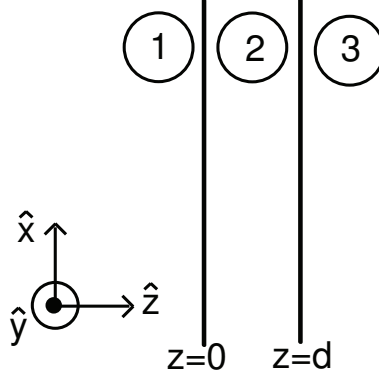


Figure 1: Infinite slab geometry used in the simulations. Region 2 is the slab having impedance η , and Regions 1 and 3 are the background having impedance η_b .

For the TE case and assuming lossless propagating fields,

$$S_z = \frac{|E_0|^2}{2Z_z}. \quad (180)$$

Using (180) in (171),

$$\begin{aligned} \langle \mathbf{F}_j \rangle_{TE} &= \hat{z} \frac{4\mu_0 S_z}{Z_z} \\ &= \hat{z} \frac{4S_z k_z}{\omega}, \end{aligned} \quad (181)$$

assuming Z_z and k_z real. For TM polarization with real Z_z , from (172),

$$\begin{aligned} \langle \mathbf{F}_j \rangle_{TM} &= \hat{z} \frac{4\mu_0 S_z Z_z}{\eta_l^2} \\ &= \hat{z} 4\mu_0 S_z \left(\frac{k_z}{\omega \epsilon_l \epsilon_0} \right) \frac{1}{\eta_l^2} \\ &= \hat{z} \frac{4S_z k_z}{\omega}. \end{aligned} \quad (182)$$

Notice that the TE pressure (181) and the TM pressure (182) with fixed S_z are identical. Consequently, it can be conjectured that the normalization used in the Jones and Leslie experiment [22] also resulted in a polarization-independent and angle-independent force.

The development of the electromagnetic force from Maxwell's equations and using the Abraham momentum leads to the important force expressions given as (94), and the simpler form for plane waves in homogeneous isotropic media in (96) that was used here to explain the Jones and Leslie experiments. The equivalent explanation of the experimental results can be built using the Lorentz force (the $q\mathbf{v} \times \mu_0 \mathbf{H}$ component, where \mathbf{v} is velocity and q is charge). A primary observation from the treatment presented here is that the measured force on a mirror can be explained using the Abraham momentum as being proportional to the refractive index of the background medium, provided the Poynting vector is constant. Therefore, the Jones and Leslie experiments do not necessarily support the validity of the Minkowski momentum. This classical picture presented here is also consistent with the measured atomic recoil being proportional to the background refractive index. One might therefore expect that the force density expressions in (94), or their relativistic forms, may explain

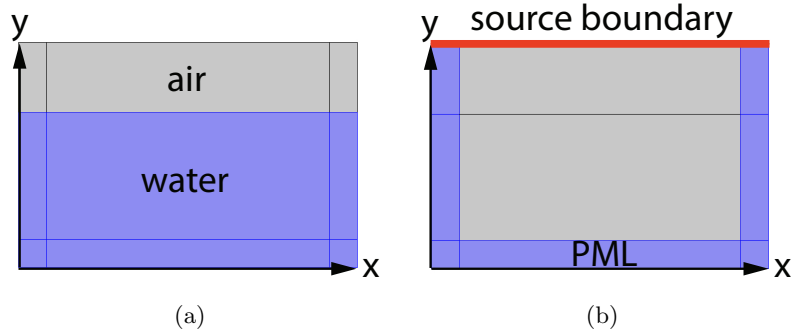


Figure 2: Figures show the 2-D simulation setup. Computational domain is divided into air part (top gray) and water part (bottom purple) in (a), and is surrounded by perfect matched layer (PML) with source boundary (red line) as in (b).

observable macroscopic forces. Of importance in a number of applications, arbitrary dispersion and loss can thus be rigorously treated. This is particularly important in the treatment of metamaterials, where the time derivative terms in (94) allow the incorporation of material dispersion for an arbitrary electromagnetic temporal field, and the anisotropy common in lattice-based metamaterials can be included in \mathbf{P} and \mathbf{M} . Provided that local homogenization applies [70], forces on dispersive structured material, even when homogenization does not hold, can thus be determined by integrating the force density.

11.2 Prediction of Ashkin’s Water Experiment

Ashkin and Dziedzic’s experiment involved radiation pressure on the surface of water and presents a landmark result related to optical force theory because it showed how the water surface moved due to the force achieved with increased optical power [71]. In their experiment, an air-water interface was illuminated with high-power (4 kW peak, maximum), 60-ns-long, 530-nm-wavelength laser pulses focused down to a spot size of radius $2\mu\text{m}$ traversing from air to water and water to air to analyze the deformation on the water surface caused by the optical force. They found that with either the light entering or exiting the water a bulge will be developed on the water surface. The direction of the bulge was initially interpreted by Ashkin and Dziedzic as evidence of recoil associated with the Minkowski form of light momentum. Subsequent analysis by Loudon showed that a Laguerre-Gaussian light beam in a dielectric will create a compressive force, giving a “toothpaste tube” effect [72], and that the radial force should create a bulge on the water surface, consistent with Ashkin’s experiment [73]. Mansuripur investigated the Lorentz and Einstein-Laub forms [45] in a dielectric slab and simulated the force distribution [44]. The results showed significant differences between the two force formulations inside the material and suggest the legitimacy of applying the Einstein-Laub force to explain Ashkin’s experiment.

We use a commercial frequency domain finite element method (FEM) solver (COMSOL) to finite the numerical field solution, and then compute the force density using the fields. Fig. 2 shows the 2-D simulation setup. Computational domain is divided into air (top gray) and water (bottom purple) as in Fig. 2 (a) and is surrounded by perfect matched layer (PML) with boundary source (red line) as in Fig. 2(b). The force is therefore calculated assuming time-harmonic, monochromatic fields, and the temporal average over a period is used to form $\langle \mathbf{f} \rangle$ from (94), as given in (210)), and (41). For convenience here, the Einstein-Laub and Lorentz time averaged force densities for non-magnetic

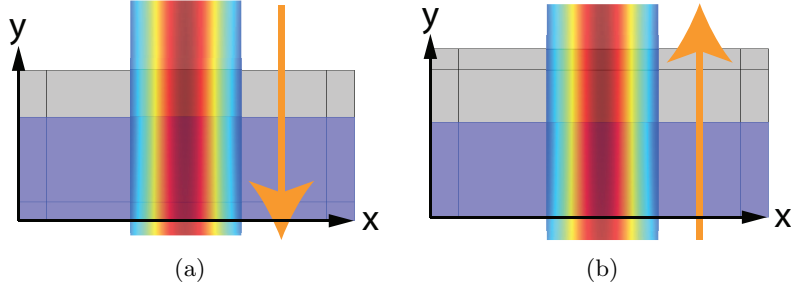


Figure 3: Adjustment of the computational domain to place the Gaussian beam focus on the water (purple) surface. The orange arrow indicates the propagation direction of the Gaussian beam. The Gaussian beam profile is generated by COMSOL with beam waist at the center. The propagation length is about half the Rayleigh range of the Gaussian beam and as a result very collimated within the range shown in the figures. (a) The beam propagating from air to water and (b) the beam propagating from water to air.

material we used in the mode are, respectively,

$$\langle \mathbf{f}_{EL} \rangle = (\hat{\mathbf{e}} \times \hat{\mathbf{h}}) \frac{\mu_0 \epsilon_0 \omega}{2} \Im \{ \chi_E E(\mathbf{r}) H^*(\mathbf{r}) \} + \frac{\epsilon_0}{2} \Re \{ (\chi_E E(\mathbf{r}) \hat{\mathbf{e}} \cdot \nabla) (\hat{\mathbf{e}} E^*(\mathbf{r})) \} \quad (183)$$

$$\langle \mathbf{f}_L \rangle = (\hat{\mathbf{e}} \times \hat{\mathbf{h}}) \frac{\mu_0 \epsilon_0 \omega}{2} \Im \{ \chi_E E(\mathbf{r}) H^*(\mathbf{r}) \} - \frac{\epsilon_0}{2} \Re \{ (\nabla \cdot \chi_E E(\mathbf{r}) \hat{\mathbf{e}}) (\hat{\mathbf{e}} E^*(\mathbf{r})) \}. \quad (184)$$

We simulated a continuous wave Gaussian beam with 530 nm wavelength and $2\mu\text{m}$ beam waist (focus) at the water surface, consistent with the experiment [71]. We considered the case with the beam incident from air to water and from water to air, as in the experiment, for the Einstein-Laub and Lorentz force expressions in (183) and (184). Earlier work by Loudon indicated that a Laguerre-Gaussian beam and a force density equivalent to Einstein-Laub should radially compress a dielectric [72] and Mansuripur simulated forces due to the Einstein-Laub and Lorentz forms in a dielectric [44], with the conclusion that the Ashkin and Dziedzic experiments support the former and not the latter. We consider an accurate numerical model of the field solution in the air-water interface region to investigate the specific forces that led to the lensing effect in the experiment.

The physical situations modeled are shown in Fig. 3, where a 2-D TM polarized Gaussian beam with out-of-plane (z axis) polarized magnetic field (H_z) is incident from air to water and from water to air in the $\mp y$ direction, respectively, with a focus on the water surface. The arrows in Fig. 3 indicate the incident directions, and the figures are from the numerical solution. The waist is not evident because of the relatively small length scale shown in the y direction.

The Gaussian beam complex field for propagation in the y direction and dominant electric field in the x direction is [74]

$$E_x(\rho, \mathbf{r}) = E_0 \frac{W_0}{W(y)} \exp \left[-\frac{\rho^2}{W^2(y)} \right] \exp \left[-jk y - jk \frac{\rho^2}{2R(y)} + j\xi(y) \right], \quad (185)$$

where $W(y) = W_0 \sqrt{1 + (y/y_0)^2}$ is the radius at which the field amplitude drops to $1/e$ of the axial value, $R(y) = y [1 + (y_0/y)^2]$ is the radius of curvature of the beam's wavefronts, $\xi(y) = \tan^{-1}(y/y_0)$ is the Gouy phase shift, an extra contribution to the phase that is seen in Gaussian beams, $W_0 = \sqrt{\lambda y_0 / \pi}$ is the beam waist size, $\rho^2 = x^2 + z^2$ is the radial distance from the beam axis, k is wave number corresponding to the material, and y_0 is the Rayleigh range where the width of the beam becomes $\sqrt{2}W_0$. We used (185) to define the incident field on the source boundary in Fig. 2(b) in

the FEM solution in 2-D (with $z = 0$). Another field component (E_y) must be from based on (185), and we draw on previous work and use the slowly varying envelope approximation [75]. The field is divergenceless, so

$$\nabla \cdot \mathbf{E} = 0 = \frac{\partial E_x}{\partial x} + \frac{\partial E_y}{\partial y}. \quad (186)$$

The slowly varying beam approximation amounts to the assumption of a y -directed partial wave, and hence

$$\frac{\partial E_y}{\partial y} \approx ikE_y. \quad (187)$$

Substituting (187) into (186) yields

$$E_y \approx \frac{i}{k} \frac{\partial E_x(x, y)}{\partial x}, \quad (188)$$

allowing us to form the vector electric field as $\mathbf{E} = \hat{\mathbf{x}}E_x + \hat{\mathbf{y}}E_y$. We note that this is not an exact solution to Maxwell's equations. However, it serves our purpose of defining a suitable beam profile for the incident field on a boundary, from which the exact (to numerical precision) solution can be computed for the scattering problem (the air-water interface in this case).

In the simulations, the electric field magnitude of the Gaussian beam and the force density (N/m^3) are normalized to the input power being 1 W. For the first case, with the Gaussian beam incident from air onto water, Fig. 4(a) shows the electric field magnitude as a function of position. The standing wave structure in the air is developed from the reflection at the air-water interface. Figures 4(b) and (c) show the time-averaged Einstein-Laub lateral force density and vertical force density, respectively from (183). From these figures we can see that the lateral force will squeeze the water to the optical axis. The vertical force tends to lift the water outward at the optical axis and press the water inward at the side lobes. One thing to be emphasized is that the lateral force is about 50 times larger than the vertical force and thus dominates the total force. This is shown in Fig. 4(d) which gives the total vector force density as a function of position in the water and clearly indicates that the forces point towards to beam axis. The force densities were integrated in the vertical (y direction) to obtain the two components of the vector pressure (lateral and vertical) and the results are given in Figs. 4(e) and (f), respectively. The pressure figures give us a clearer picture of the force acting on the water surface and make it clear that lateral and vertical pressure would together form a bulge at the water surface. This results in the lens effect that moves the focus into the water with increasing optical power that was observed by Ashkin and Dziedzic [71].

We used the numerical field solution in the Lorentz force density expression in (184), and those results are given in Fig. 5. In this case, the lateral Lorentz force would split the water from the optical axis, as shown in Fig. 5(a). From Fig. 5(b), the vertical Lorentz force acts exactly the opposite direction to the Einstein-Laub force, pressing the water inward at the center but lifting the water up at the side lobes. The Lorentz lateral force is about 50 times larger than the vertical force and as a result the total force, shown in Fig. 5(c) points mostly outward from the center. The pressure obtained from force density shown in Figs. 5(d) and (e) demonstrate that a depression on the water surface would be formed. This prediction contradicts the data from Ashkin and Dziedzic [71].

Next we investigate the second case when the Gaussian beam is illuminating from water to air. Because of the reflection from the air-water interface, there are standing wave patterns inside the water, as shown in Fig. 6(a). Consequently, the Einstein-Laub lateral force and vertical force densities shown in Figs. 6(b) and (c) show periodic structure. The vertical force density is about an order of magnitude larger than the lateral force. This notable distinction from the case with illumination from air to water is presumably related to the standing wave structure in the water. The total force give in Fig. 6(d) shows that there is a vertical compression and stretching of the water as a

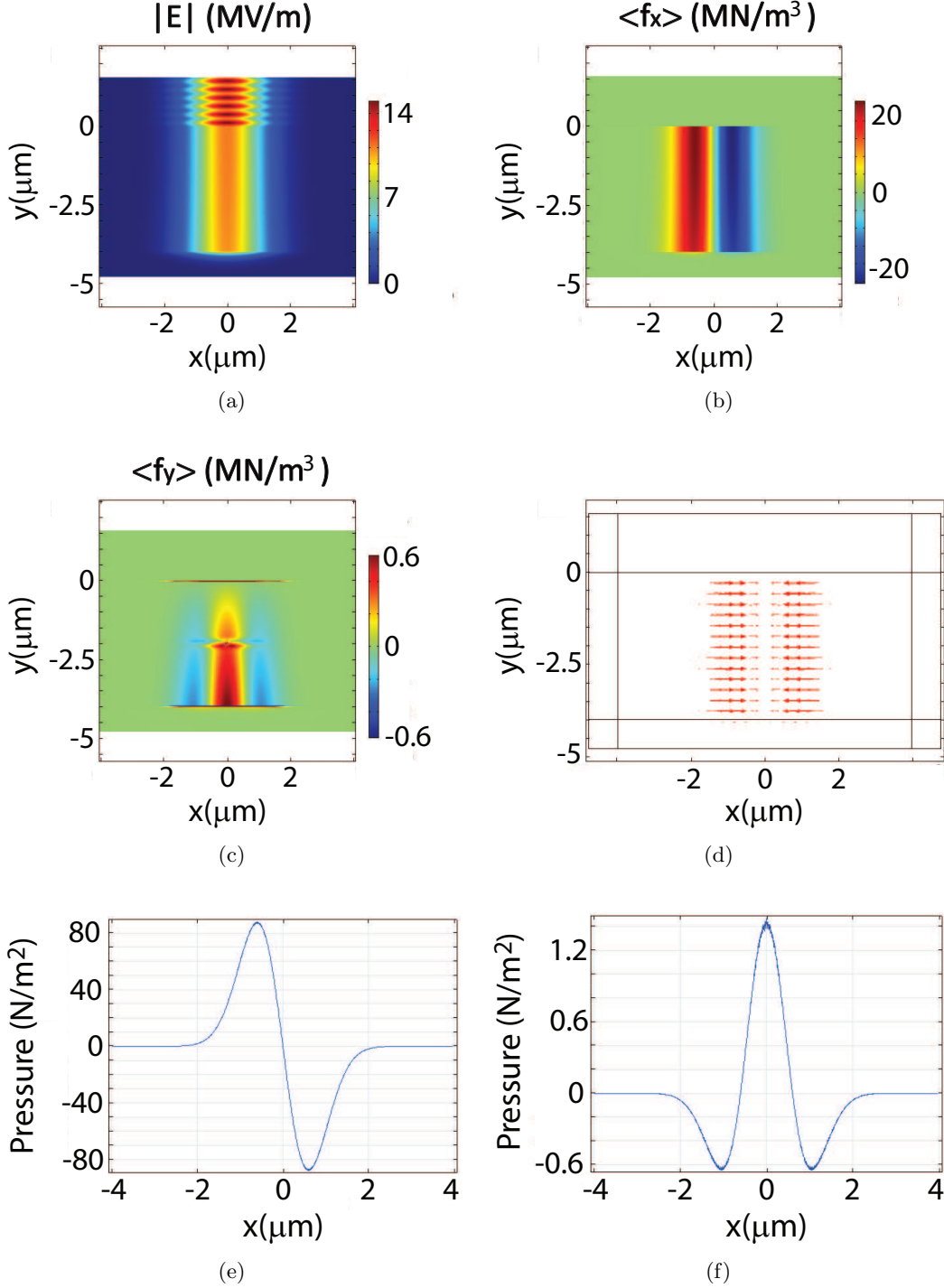


Figure 4: (a) The TM (H_z) polarized Gaussian beam electric field magnitude with illumination from air to water. Time-averaged Einstein-Laub force density (N/m^3) distribution is shown separately in lateral direction $f_x \hat{x}$ (b), and in vertical direction $f_y \hat{y}$ (c). The total force $\mathbf{f} = f_x \hat{x} + f_y \hat{y}$ is demonstrated in (d) by arrows indicating the direction. The pressure obtained by integrating along the vertical axis (y axis) on both lateral force density and vertical force density are shown in (e) and (f), respectively.

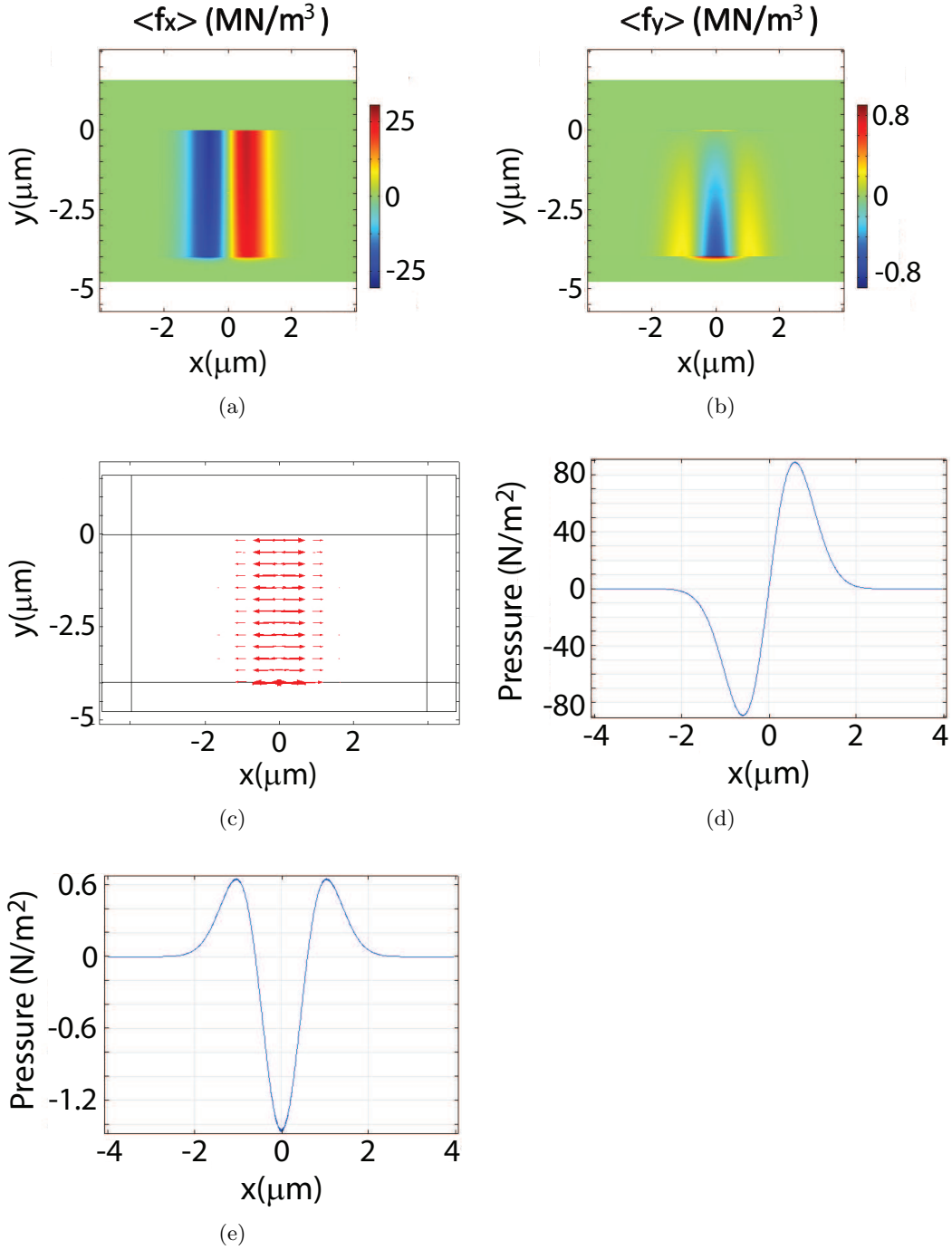


Figure 5: The Lorentz force density distribution when a TM (H_z) polarized Gaussian beam illuminates from air to water. The time-averaged Lorentz force density (N/m³) distribution shown separately in lateral direction $f_x \hat{\mathbf{x}}$ (a), and in the vertical direction $f_y \hat{\mathbf{y}}$ (b). The total force $\mathbf{f} = f_x \hat{\mathbf{x}} + f_y \hat{\mathbf{y}}$ is given in (c) by arrows indicating the direction. The pressure obtained by integrating along the vertical axis (y axis) for both the lateral force density and vertical force density are shown in (d) and (e), respectively.

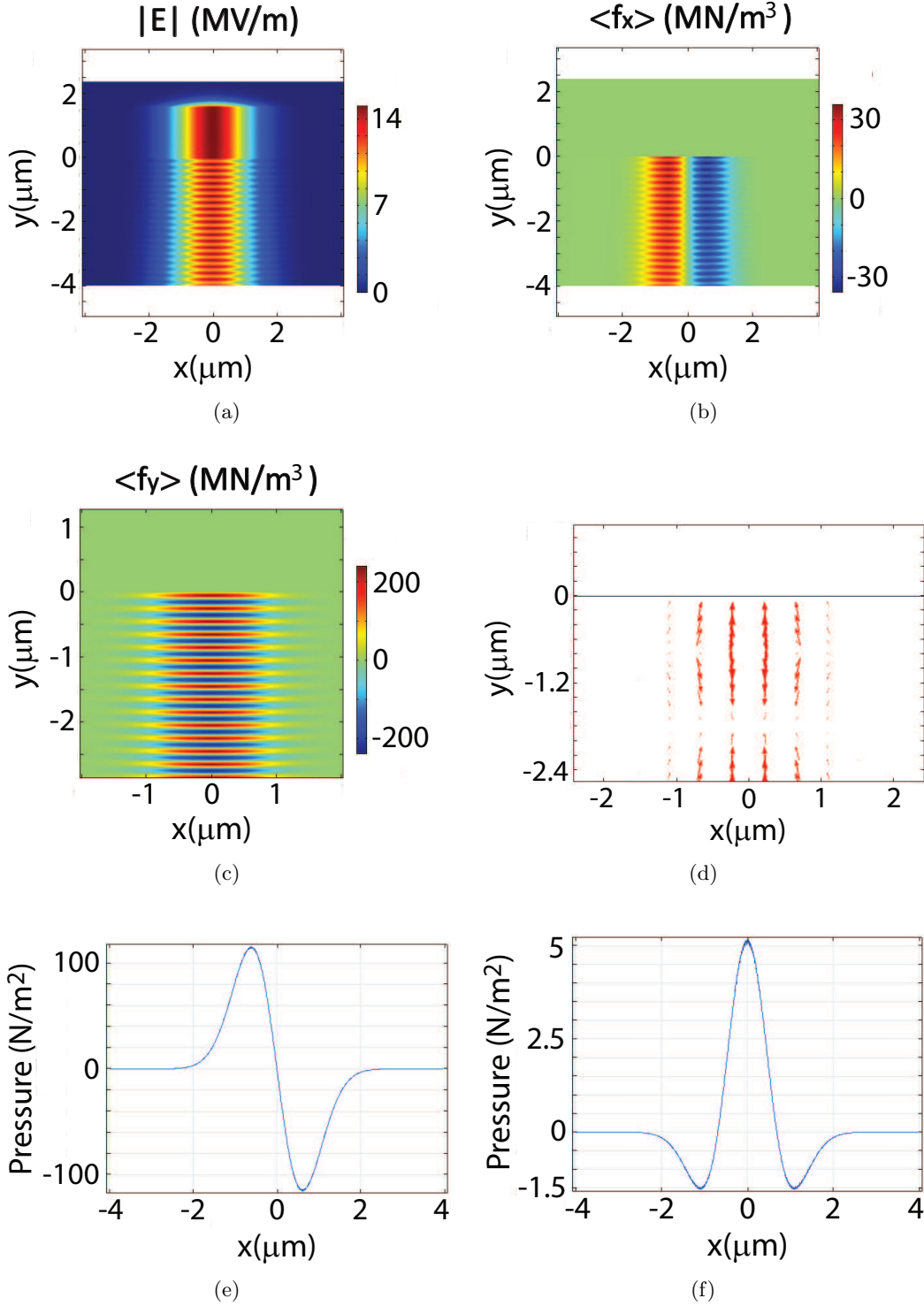


Figure 6: (a) The TM (H_z) polarized Gaussian beam electric field magnitude with illumination from water to air. The time-averaged Einstein-Laub force density (N/m^3) distribution is shown separately in the lateral direction $f_x \hat{\mathbf{x}}$ (b), and in vertical direction $f_y \hat{\mathbf{y}}$ (c). The total force $\mathbf{f} = f_x \hat{\mathbf{x}} + f_y \hat{\mathbf{y}}$ is demonstrated in (d) by arrows indicating the direction. The pressure obtained by integrating along the vertical direction (y axis) the lateral force density and the vertical force density are shown in (e) and (f), respectively.

function of depth and position in the standing wave. However, note that the net force near to the surface is upward. Also, the pressure obtained by integrating force density over depth, shown in Figs. 6(e) and (f), clearly shows a compression a lift. Note that the vertical pressure is larger than the lateral pressure in this case, and that there are side lobes in Fig. 6(f) that may play an interesting role because there amplitude is significant relative tot he lateral pressure shown in Fig. 6(e). Our conclusion is the a bulge will result, and the prediction is again consistent with the measurements of Ashkin and Dziedzic [71].

Now consider the force predicted by the Lorentz expression with illumination from water to air. The results we found are given in Fig. 7. The Lorentz force densities in Figs. 7(a) and (b) also have a periodic structure because of the reflection from the water-air interface. From Fig. 7(c), there are compressive and stretching total force densities inside the water as a function of position. Figures 7(d) and (e) show the lateral pressure and a nonzero value of vertical pressure on the water, respectively. From both pressure contributions it is clear that a depression on the surface of the water would be form.

For either light is illuminating from air to water, the first case, or from water to air, the second case, the simulation results show that the Einstein-Laub force is consistent with the Ashkin and Dziedzic experiments and the Lorentz form is not. Our numerical analysis therefore strongly suggests that the Einstein-Laub force is the correct way to simulate this experiment. By determining the correct force we should note that the Abraham momentum was used.

11.3 Prediction of Atom Recoil Momentum Experiment

The recoil momentum of an atom after absorption of a photon has been measured to be $\hbar k_0 n$, where k_0 is the vacuum wave number and n the background refractive index [25]. While force relates to change in momentum, this does convey a strong case for use of the Minkowski form of momentum.

We consider a very thin dielectric slab as a simple analytical model. At the atomic level, scatter corresponds to absorption and re-emission of a photon, and an array of atoms in a sheet provides for a simple picture. We develop an expression for pressure based on the Einstein-Laub form of the force density and with the Abraham momentum. We show that the force on the thin sheet is proportional to the background refractive index, thereby predicting the result from theory for the first time.

Associating the Abraham form of the electromagnetic momentum ($\mathbf{g}_A = \mathbf{E} \times \mathbf{H}/c^2$, with c the speed of light in vacuum) with the electromagnetic energy in nondispersive media yields the single photon momentum magnitude of $\hbar k_0/n$, where n is refractive index, $\hbar = h/2\pi$, with h being Planck's constant, and k_0 is the free space wave number ($k_0 = \omega/c$, with $c = 1/\sqrt{\mu_0\epsilon_0}$). Doing likewise with the Minkowski momentum ($\mathbf{g}_M = \mathbf{D} \times \mathbf{B}$) gives a momentum of $n\hbar k_0$. Atoms have been measured to have a recoil momentum of $n\hbar k_0$ [25], important in atom interferometry with optical gratings and consistent with the deBroglie momentum. This result appears to suggest that \mathbf{g}_M is the correct description of photon momentum. However, mechanical momentum is imparted by the photon or field with some force, and that force gives rise to a time-rate of change in mechanical momentum. Our task is to consider the force that gives rise to this momentum, and we do so here with an example that is relevant for this experimental result.

We described the force/pressure on a dielectric slab in a background using the Einstein-Laub force for a normally incident plane wave [57], which from (96) with no impressed current or surface current becomes

$$\mathbf{f} = \frac{\partial \mathbf{P}}{\partial t} \times \mu_0 \mathbf{H} - \frac{\partial \mu_0 \mathbf{M}}{\partial t} \times \epsilon_0 \mathbf{E}, \quad (189)$$

We consider a slab of thickness d and complex impedance $\eta = \eta' + i\eta''$, with normal \hat{z} , as in Fig. 1. For simplicity, the background Regions 1 and 3 (in Fig. 1) are assumed to have the same material

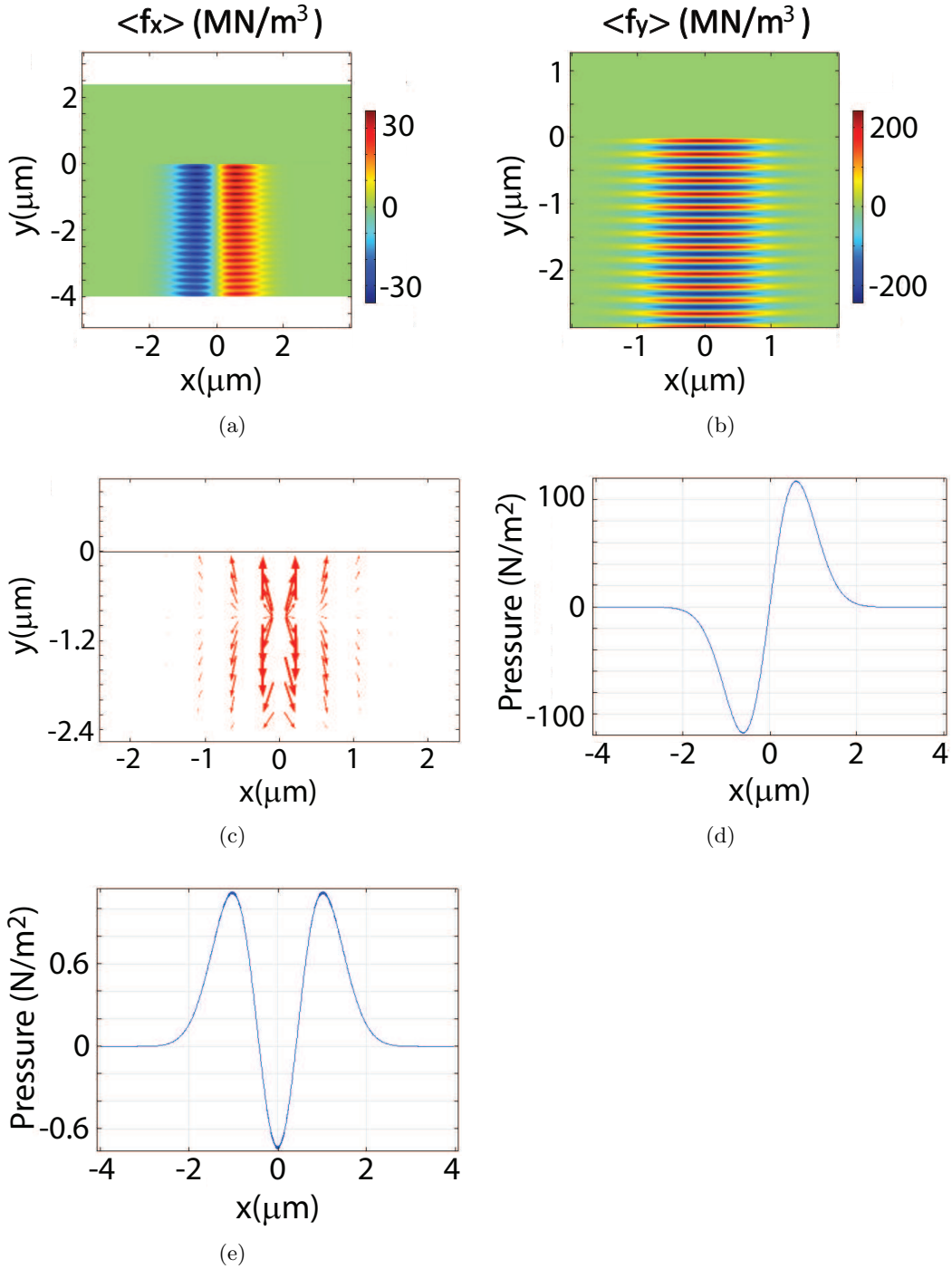


Figure 7: The Lorentz force density distribution when a TM (H_z) polarized Gaussian beam is incident from water to air. The time-averaged Lorentz force density (N/m³) distribution is shown separately in the lateral direction $f_x \hat{\mathbf{x}}$ (a), and in the vertical direction $f_y \hat{\mathbf{y}}$ (b). The total force $\mathbf{f} = f_x \hat{\mathbf{x}} + f_y \hat{\mathbf{y}}$ is indicated in (c) by arrows as a function of position. The pressure obtained by integrating along the vertical direction (y axis) for the lateral force density and vertical force density are shown in (d) and (e), respectively.

properties, with complex impedance $\eta_b = \eta'_b + i\eta''_b$. A monochromatic plane wave propagating in the \hat{z} -direction is considered normally incident on the slab from the left, giving fields in each region of the form

$$\mathbf{E} = -\hat{\mathbf{y}} \Re [E(z, \omega_0) e^{-i\omega_0 t}] \quad (190)$$

$$\mathbf{H} = \hat{\mathbf{x}} \Re [H(z, \omega_0) e^{-i\omega_0 t}]. \quad (191)$$

Defining the complex electric and magnetic susceptibilities as $\chi_E = \chi'_E + i\chi''_E$ and $\chi_H = \chi'_H + i\chi''_H$, respectively, we write

$$\mathbf{P} = -\hat{\mathbf{y}} \epsilon_0 \Re [\chi_E(\omega_0) E(z, \omega_0) e^{-i\omega_0 t}] \quad (192)$$

$$\mathbf{M} = \hat{\mathbf{x}} \Re [\chi_H(\omega_0) H(z, \omega_0) e^{-i\omega_0 t}]. \quad (193)$$

Substituting \mathbf{E} , \mathbf{P} , \mathbf{H} and \mathbf{M} into (189) and taking the time average over the carrier period $t_0 = 2\pi/\omega_0$, we obtain

$$\langle \mathbf{f} \rangle = \hat{\mathbf{z}} \frac{\mu_0 \epsilon_0 \omega_0}{2} \Im [(\chi_E - \chi_H^*) E H^*], \quad (194)$$

where \Im is the imaginary part and the scalar fields (E and H) are the total complex fields.

Referring to Fig. 1 and assuming an incident electric field $E_0 \exp(ik_1 z)$, where $k_1 = k'_1 + ik''_1$ is the wave number in Region 1, the exact plane wave solution upon imposition of the boundary conditions gives the fields inside the slab as

$$E = 2\eta E_0 \left[\frac{(\eta_b + \eta) e^{ik(z-d)} + (\eta_b - \eta) e^{-ik(z-d)}}{(\eta_b + \eta)^2 e^{-ikd} - (\eta_b - \eta)^2 e^{ikd}} \right] \quad (195)$$

$$H = 2E_0 \left[\frac{(\eta_b + \eta) e^{ik(z-d)} - (\eta_b - \eta) e^{-ik(z-d)}}{(\eta_b + \eta)^2 e^{-ikd} - (\eta_b - \eta)^2 e^{ikd}} \right], \quad (196)$$

where E_0 is the incident electric field amplitude in Region 1 at $z = 0$ and $k = k' + ik''$ is the complex wave number in the slab (Region 2). Equations (195) and (196) provide the exact time-harmonic (steady state) field solutions, accounting for all reflections. Using (195) and (196) in (194), we find

$$\begin{aligned} \langle \mathbf{f} \rangle = \hat{\mathbf{z}} & \frac{2\mu_0 \epsilon_0 \omega_0 E_0^2}{|(\eta_b + \eta)^2 e^{-ikd} - (\eta_b - \eta)^2 e^{ikd}|^2} \\ & \left\{ 2 [(\chi'_E - \chi'_H) \eta' - (\chi''_E + \chi''_H) \eta''] \right. \\ & \left[2 (\eta''_b \eta' - \eta'_b \eta'') \cos [2k'(z-d)] \right. \\ & \left. + (|\eta|^2 - |\eta_b|^2) \sin [2k'(z-d)] \right] \\ & \left. + [(\chi'_E - \chi'_H) \eta'' + (\chi''_E + \chi''_H) \eta'] \right. \\ & \left. \left[|\eta_b + \eta|^2 e^{-2k''(z-d)} - |\eta_b - \eta|^2 e^{2k''(z-d)} \right] \right\}. \quad (197) \end{aligned}$$

Note that $\langle \mathbf{f} \rangle$ in (197) depends on the impedance of the background and not the sign of its refractive index. When $\eta_b = \eta$ (the impedance of the background and slab are the same, or in the absence of the slab), the force density becomes

$$\langle \mathbf{f} \rangle = \hat{\mathbf{z}} \frac{\mu_0 \epsilon_0 \omega_0 E_0^2}{2|\eta|^2} [(\chi'_E - \chi'_H) \eta'' + (\chi''_E + \chi''_H) \eta'] e^{-2k''z}, \quad (198)$$

consistent with that in homogeneous media for the monochromatic light in our previous work [16]. Note that $\langle \mathbf{f} \rangle$ in (198) will be positive (negative) for a medium having overall loss (gain). An example arrangement having $\eta_b = \eta$ is a negative index slab with $\mu = \epsilon$ placed in vacuum.

The total time-averaged force per unit area for the slab can then be found by integrating $\langle \mathbf{f} \rangle$ in (197) over the total slab, giving

$$\begin{aligned} \langle \mathbf{F} \rangle &= \int_0^d \langle \mathbf{f} \rangle dz = \hat{z} \frac{2\mu_0\epsilon_0\omega_0 E_0^2}{|(\eta_b + \eta)^2 e^{-ikd} - (\eta_b - \eta)^2 e^{ikd}|^2} \\ &\quad \left\{ 2 [(\chi'_E - \chi'_H) \eta' - (\chi''_E + \chi''_H) \eta''] [2(\eta'_b \eta' - \eta'_b \eta'')] \right. \\ &\quad \times \left. \frac{\sin(2k'd)}{2k'} + (|\eta|^2 - |\eta_b|^2) \frac{\cos(2k'd) - 1}{2k'} \right] \\ &\quad + [(\chi'_E - \chi'_H) \eta'' + (\chi''_E + \chi''_H) \eta'] \\ &\quad \left. \left[|\eta_b + \eta|^2 \frac{e^{2k''d} - 1}{2k''} - |\eta_b - \eta|^2 \frac{1 - e^{-2k''d}}{2k''} \right] \right\}. \end{aligned} \quad (199)$$

Note that (199) is not valid when $k' = 0$ or $k'' = 0$, because of the singularities. In these limiting cases, $\langle \mathbf{F} \rangle$ must be evaluated by taking the proper limits, $\lim_{k' \rightarrow 0} \langle \mathbf{F} \rangle$ and $\lim_{k'' \rightarrow 0} \langle \mathbf{F} \rangle$.

Consider a simple case where the constitutive parameters are real and both η and η_b are real. From (197), the time average force density becomes

$$\langle \mathbf{f} \rangle = \hat{z} \frac{\omega_0\mu_0\epsilon_0 E_0^2 (\chi'_E - \chi'_H) \eta' (|\eta'|^2 - |\eta'_b|^2) \sin[2k'(z-d)]}{[4\eta'^2 \eta_b'^2 \cos^2(k'd) + (\eta_b'^2 + \eta'^2)^2 \sin^2(k'd)]}, \quad (200)$$

and upon integrating over the slab thickness, the total time-averaged force per unit area on the slab is

$$\langle \mathbf{F} \rangle = \hat{z} \frac{\omega_0\mu_0\epsilon_0 E_0^2 (\chi'_E - \chi'_H) \eta' (|\eta'|^2 - |\eta'_b|^2) [\cos(2k'd) - 1]}{[4\eta'^2 \eta_b'^2 \cos^2(k'd) + (\eta_b'^2 + \eta'^2)^2 \sin^2(k'd)] 2k'}. \quad (201)$$

In this special case (ϵ , μ , η and η_b all are real), $\langle \mathbf{F} \rangle$ could be either positive or negative, depending on whether $(1 - \mu'/\epsilon')(\eta_b'^2 - \eta'^2)$ is positive or negative. Equation (201) shows that the total force on a lossless dielectric slab placed in vacuum will always be positive (or zero if the slab thickness is an integral multiple of $\lambda/2$, where λ is the wavelength in the slab). Note that in the special case where $\epsilon' = \mu'$ and $\epsilon'' = \mu'' = 0$, both $\langle \mathbf{f} \rangle$ and $\langle \mathbf{F} \rangle$ will be zero, irrespective of the background medium (such as for a negative index slab having $\epsilon = \mu = -1$). We note that previous numerical simulations of the force on an example semi-infinite negative index medium found a positive (pushing) force [30]. This is consistent with observations of the force on a negative index slab, or on a positive index material in a negative index background, based on (201).

Now consider a very thin, lossless slab in a lossless background, with $\epsilon > \epsilon_b$, and no magnetic materials. From (201), the pressure is

$$\langle \mathbf{F} \rangle = \hat{z} \frac{\omega_0\mu_0\epsilon_0 E_0^2 (\chi_E) \eta (\eta^2 - \eta_b^2) [\cos(2kd) - 1]}{[4\eta^2 \eta_b^2 \cos^2(kd) + (\eta_b^2 + \eta^2)^2 \sin^2(kd)] 2k}. \quad (202)$$

Using the small argument approximations $\sin x \approx x$ and $\cos x \approx 1 - x^2/2$, (202) becomes

$$\begin{aligned} \langle \mathbf{F} \rangle &\approx \hat{z} \frac{\omega_0\mu_0\epsilon_0 E_0^2 (\epsilon - 1) \frac{\eta_0}{\sqrt{\epsilon}} \left(\frac{\eta_0^2}{\epsilon} - \frac{\eta_0^2}{\epsilon_b} \right) \left[-\frac{(2kd)^2}{2} \right]}{\left[4 \frac{\eta_0^2}{\epsilon} \frac{\eta_0^2}{\epsilon_b} (1 - (kd)^2) + \left(\frac{\eta_0^2}{\epsilon} + \frac{\eta_0^2}{\epsilon_b} \right)^2 (kd)^2 \right] 2k} \\ &\approx \hat{z} \frac{\omega_0\mu_0\epsilon_0 E_0^2 (\epsilon - 1) \frac{\eta_0}{\sqrt{\epsilon}} \left(\frac{\eta_0^2}{\epsilon} - \frac{\eta_0^2}{\epsilon_b} \right) \left[-\frac{(2kd)^2}{2} \right]}{\left[4 \frac{\eta_0^2}{\epsilon} \frac{\eta_0^2}{\epsilon_b} \right] 2k} \\ &\approx \hat{z} \frac{k_0^3 E_0^2 d^2}{4\omega\eta_0} [\epsilon\epsilon_b(\epsilon - 1)(\epsilon_b - \epsilon)]. \end{aligned} \quad (203)$$

We set $\epsilon = \epsilon_b + \delta$ in (203), where δ is a perturbational parameter, giving

$$\begin{aligned}\langle \mathbf{F} \rangle &\approx \hat{\mathbf{z}} \frac{k_0^3 E_0^2 d^2}{4\omega\eta_0} (\delta\epsilon_b + \delta^2 - \delta) \\ &\approx \hat{\mathbf{z}} \left[\frac{k_0^3 E_0^2 d^2}{4\omega\eta_b} \right] \delta\sqrt{\epsilon_b}\end{aligned}\quad (204)$$

Equation (204) can be couched in a more insightful form in relation to a relevant experiment [25]. Write the Poynting vector as

$$\begin{aligned}S &= \frac{E_0^2}{2\eta_b} \\ &= \hbar\omega R,\end{aligned}\quad (205)$$

where R is the number of photons per second per m^2 . Substituting (205) into (204) and rearranging yields

$$\langle \mathbf{F} \rangle \approx \hat{\mathbf{z}} \frac{R}{2} \left(k_0 \sqrt{\delta} d \right)^2 [\hbar k_0 n_b], \quad (206)$$

where in this case $n_b = \sqrt{\epsilon_b}$. The unit-less term in the curved braces describes the strength of scatter. The term in square brackets is the Minkowski momentum. The force on the thin dielectric slab is in agreement with measurement of the atom recoil after having absorbed a photon being proportional to the background refractive index. Our point is that this result follows from use of a field formulation and the Abraham momentum. The factor of 1/2 in (206) presumably relates to the geometry and symmetry.

12 Additional Contribution - Pressure Enhancement from a Structured Metal Surface

We utilize a force description that we have discussed in our previous work [16, 57, 61] that has been developed by Penfield and Haus [6] and is consistent with the Einstein and Laub form [1]. Using this description, the electromagnetic kinetic force density in material media becomes

$$\begin{aligned}\mathbf{f} &= \frac{\partial \mathbf{P}}{\partial t} \times \mu_0 \mathbf{H} - \frac{\partial \mu_0 \mathbf{M}}{\partial t} \times \epsilon_0 \mathbf{E} + \rho \mathbf{E} \\ &\quad - \mu_0 \mathbf{H} \times \mathbf{J} + (\mathbf{P} \cdot \nabla) \mathbf{E} + \mu_0 (\mathbf{M} \cdot \nabla) \mathbf{H},\end{aligned}\quad (207)$$

with \mathbf{f} having SI units of N/m^3 and \mathbf{P} the polarization, \mathbf{M} the magnetization, \mathbf{J} the free electric current density, ρ the free electric charge density, ϵ_0 the permittivity of free space, and μ_0 the permeability of free space. In our special case, the free current and free charge densities will both be zero, and we also assume there is no magnetic material response, so the terms involving \mathbf{M} in (207) are zero. Consequently, one term in (207) describes the radiation pressure, $\partial \mathbf{P} / \partial t \times \mu_0 \mathbf{H}$, and one the gradient force, $(\mathbf{P} \cdot \nabla) \mathbf{E}$. Our interest here is the force that can be exerted on a structured metal surface by laser light, and from (207), the force density within the metal becomes

$$\mathbf{f} = \frac{\partial \mathbf{P}}{\partial t} \times \mu_0 \mathbf{H} + (\mathbf{P} \cdot \nabla) \mathbf{E}. \quad (208)$$

We consider a time-harmonic, monochromatic field with frequency dependence $\exp(-i\omega t)$ and an isotropic dielectric response, giving $\mathbf{P}(\mathbf{r}, \omega) = \epsilon_0 \chi_E(\mathbf{r}, \omega) \mathbf{E}(\mathbf{r}, \omega)$, with χ_E the electric susceptibility

(and dielectric constant $\epsilon = 1 + \chi_E$). With the frequency domain implied, the polarization can then be written as

$$\mathbf{P}(\mathbf{r}, t) = \hat{\mathbf{e}}\epsilon_0\Re[\chi_E(\mathbf{r})E(\mathbf{r})e^{-i\omega t}], \quad (209)$$

where $\hat{\mathbf{e}}$ is a unit vector, E is the phasor electric field, and where $\Re\{\cdot\}$ is the real part. By defining \mathbf{E} and \mathbf{H} similarly, the time average of the force density in (208) becomes

$$\begin{aligned} \langle \mathbf{f} \rangle = & (\hat{\mathbf{e}} \times \hat{\mathbf{h}}) \frac{\mu_0 \epsilon_0 \omega}{2} \Im\{\chi_E E(\mathbf{r}) H^*(\mathbf{r})\} \\ & + \frac{\epsilon_0}{2} \Re\{(\chi_E E(\mathbf{r}) \hat{\mathbf{e}} \cdot \nabla)(\hat{\mathbf{e}} E^*(\mathbf{r}))\}, \end{aligned} \quad (210)$$

where $\Im\{\cdot\}$ is the imaginary part. Following a numerical solution for the fields, we use (210) to obtain the time-averaged force density, and then form the pressure by integrating the y -component of the force density over the depth of the structure as $\langle p_y \rangle = \int_y \langle f_y \rangle dy$, with units of N/m^2 .

Consider the two structured Au metal films in Fig. 8 with free space above and below. A 2D numerical finite element method solution [76] for the fields used periodic boundary conditions on the left and right and assumed a plane wave normally incident from above with E_x, H_z (note the coordinate system in the lower left of each figure). The top and bottom surfaces of the simulation domain were implemented as port boundaries so that the scattered waves are absorbed to simulate semi-infinite domains. A wavelength of 633 nm was used and the complex dielectric constant for Au was taken from the literature [77]. We studied the arrangement of Fig. 8 with 30 nm and 60 nm wide slots of varying depths, as well as a sawtooth geometry. With the polarization considered, plasmonic cavity modes can form in the slot [78]. We analyzed a number of structures to evaluate the influence of a nanostructured surface on the optical force experienced by the sample. In order to consider a situation representative of an experiment, the Poynting vector of the incident plane wave was normalized for an illumination power density equivalent to 1 mW over a uniformly illuminated circular spot size of diameter 1 μm .

For the slot geometry of Fig. 8, we solved for the fields for slot widths (W) of 30 nm and 60 nm, and depths (D) ranging from 1 nm to 90 nm, in steps of 1 nm. We calculated the average force density from (210) using the numerical solutions for the fields, and upon integration over the thickness of the film, found the pressure on the Au film, $\langle p_y \rangle$. Plots of the y -component of force density, $\langle f_y \rangle$, are given in Fig. 9 for a 30 nm wide slot and slot depths of 1, 51, and 81 nm. Notice that the force distribution varies considerably as a function of slot depth.

In order to develop a better picture of the relative force enhancement as a function of slot geometry, Fig. 9(d) gives the pressure, $\langle p_y \rangle$, for the 30 nm and 60 nm slot widths as a function of

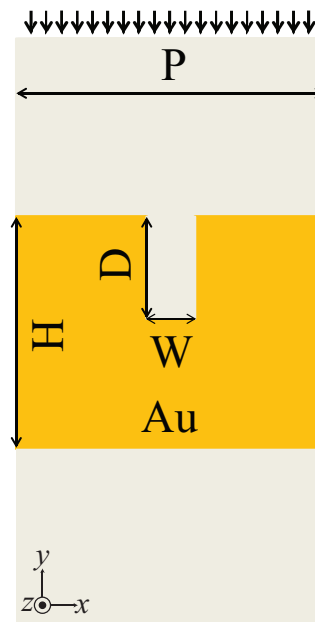


Figure 8: Simulated gold (Au) metal film structures in free space: D is varied between 1 nm and 90 nm, with W set to 30 nm and 60 nm. In all cases, the Au sample is illuminated from the top by 633 nm light (E_x, H_z), P is 400 nm, H is 200 nm. Periodic boundary conditions are enforced on the left and right, are port boundaries are on the top and bottom.

slot depth with a (normalized) input power density of 1 W/m^2 . The maximum pressure occurs at the resonant depth, and the peak pressure is higher for the 30 nm slot case. The resonant 30 nm slot in Au at 633 nm results in approximately a 23-fold enhancement in pressure.

Consider the simple approximation where the planar Au surface is treated as a perfect electric conductor (PEC), which assumes that the imaginary part of the dielectric constant approaches minus infinity or, equivalently, that the real part approaches plus infinity. Consequently, the skin depth goes to zero and the total field in the incident half-space has zero tangential electric field and a maximum in the magnetic field. The radiation pressure on this surface becomes [69]

$$\langle p_y \rangle = \frac{4S_{-y}k}{\omega} = \frac{4S_{-y}}{c}, \quad (211)$$

where S_{-y} is the incident power density (Poynting vector magnitude in the $-y$ -direction), k is the (free space, in this case) wave number, and c is the speed of light in vacuum. Normalizing to $S_{-y} = 1 \text{ W/m}^2$, we find an analytical macroscopic pressure of $1.33 \times 10^{-8} \text{ N/m}^2$ on the PEC. The value we found through simulation for a planar Au (with $\epsilon = -11.82 + i1.23$) surface was $1.29 \times 10^{-8} \text{ N/m}^2$, which is the zero slot depth result in Fig. 9(d).

To ascertain the primary mechanism by which this force enhancement occurs, consider a decomposition of the pressure into two components, one corresponding to the radiation pressure term, or cross term, in (208) and the other to the spatially varying electric field term, or divergence term. Far from resonance, the term associated with radiation pressure dominates. This is because there is relatively little spatial variation of the field. As can be seen in Fig. 9(a), where the surface is almost perfectly planar, the force density is significant within about one skin depth of the surface. As resonance is approached, the magnitude of the fields in the cavity increase, as does the spatial variation of the field, leading to an increase in the divergence term, as in Fig. 9(b). At resonance, the divergence component dominates, and is thus primarily responsible for the significant force enhancement. Further analysis of Fig. 9(b) shows an enhancement of the force density near the top surface when the slot is resonant. We interpret this to be due to the more efficient excitation of the surface wave on the top surface of the metal film when the cavity is resonant, and that this surface wave contributes to the pressure on the film, thus yielding an increase in the radiation pressure term as well.

By conservation of momentum, the greatest momentum an electromagnetic wave could impart is twice the incident momentum, which would happen in the case of total reflection. This momentum exchange has been measured to depend of the refractive index of the background [25]. The kinetic force density, as described by (207), depends on both the spatial variation of the fields and the homogenized material parameters. As we have demonstrated, it is possible to substantially enhance the total force through control of the nanostructure. It should be noted that this does not inherently violate conservation of momentum, as momentum and force are interrelated, but distinct. It is presumably also possible to further control the force through the material properties, the sign of the real part of the dielectric constant (metal or dielectric), and the imaginary part (loss or gain [16]). Also, one could potentially use magnetic materials to further enhance the force density, thereby including the two magnetization terms in (207) that we disregarded.

Pressure Example: We estimate the radiation pressure and y -directed force on a perfect reflector and a Au membrane with nanoslots for conditions easily implemented in our experiments. Consider the simple approximation where the planar Au surface is treated as a perfect electric conductor (PEC), or a perfect reflector, and use of (211) [69]. We found a pressure of $1.33 \times 10^{-8} \text{ W/m}^2$ with an incident power density of 1 W/m^2 . For a 1 mW laser uniformly illuminating a flat Au surface with area $10\mu\text{m} \times 100\mu\text{m}$, the intensity will be 10^6 W/m^2 . The force over the surface will then be 13.3 pN. Using our example of an Au film with resonant slots in Fig. 9, we can determine the

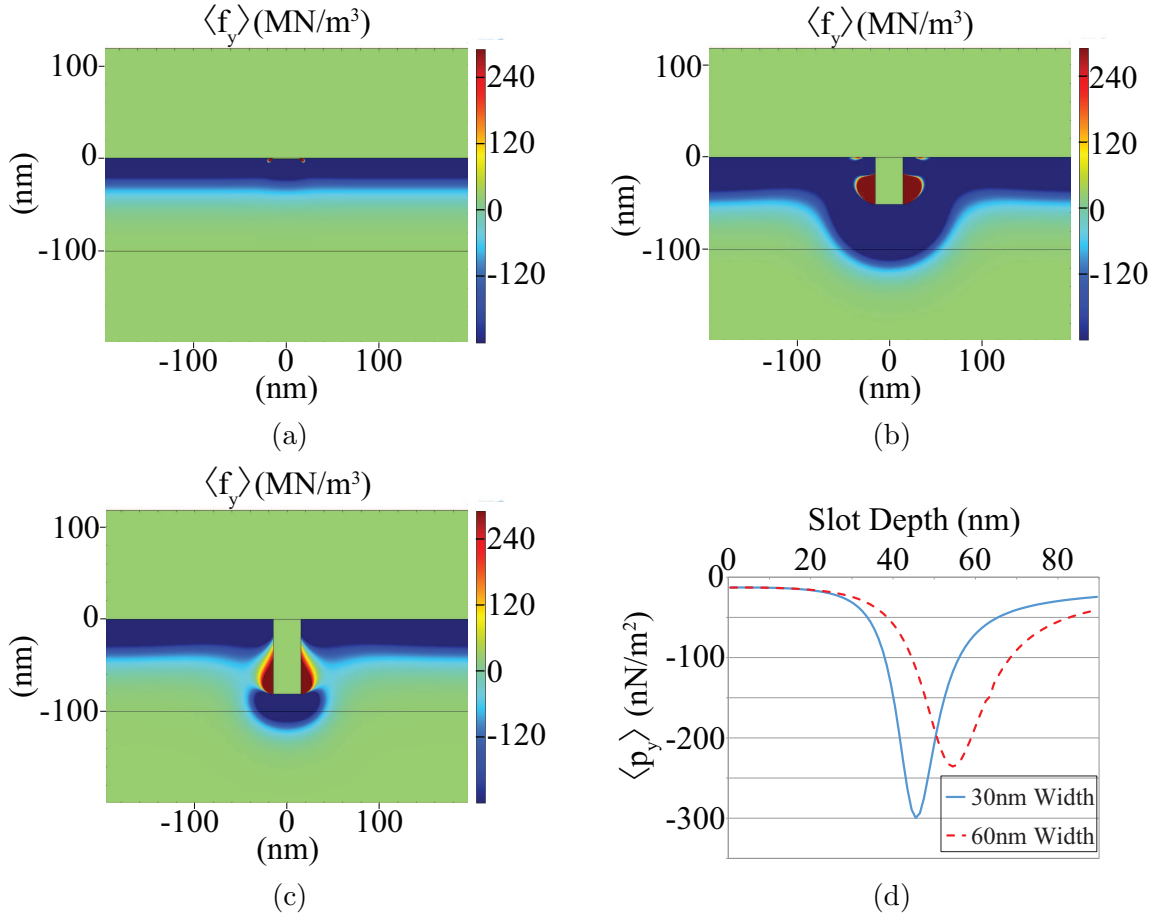


Figure 9: The y -component of the force density for the 30 nm wide slot at various slot depths: (a) 1 nm; (b) 51 nm; (c) 81 nm. The simulation has an incident power density equivalent to 1 mW of 633 nm laser illumination over a circular spot of diameter 1 μm . For reference, resonance is achieved at about 46 nm for the 30 nm wide slot. (d) Numerical results for the pressure as a function of slot depth in a Au film for the two slot widths, calculated for slot depths from 1 nm to 90 nm in 1 nm steps and $\langle p_y \rangle$, in N/m^2 determined by integrating the y -component of force density over the depth of the Au nanostructure. These values are normalized to a Poynting vector power density of $1 \text{ W}/\text{m}^2$ and the wavelength is 633 nm.

relative increase in pressure due to the slots. Consider that the slots are distributed as in Fig. 8 along the longer dimension. For case in Fig. 8, with a 400 nm period, each 30 nm slot offers a pressure enhancement of 23. The total force on the Au membrane with the slots therefore becomes a huge 306 pN.

13 Conclusion

Kinetic force information is not incorporated into Maxwell's equations and therefore requires additional information that has raised issues related to the representation of electromagnetic effects within a rigorous kinetic description. The correct formulation may depend on the circumstances and, given these, it is possible there is more than one path to the single form that can describe experiments. Careful experiments then become the benchmark by which theory must be measured. Presumably at the most general level, with the restrictions implied in Maxwell's equations and the non-relativistic case considered, an effective theory should be capable of describing the results in all relevant experiments.

There are really three viable force density representations developed here: (41), (94), and (117). Comparisons are thus in order at this point. However, we should note that the Einstein-Laub form (94) is on the stronger physical ground.

The non-magnetic forms of (41), (88), and (94), for comparison, are

$$\mathbf{f}_{LE} = \frac{\partial \mathbf{P}}{\partial t} \times \mu_0 \mathbf{H} + \rho \mathbf{E} - \mu_0 \mathbf{H} \times \mathbf{J} - (\nabla \cdot \mathbf{P}) \mathbf{E} \quad (212)$$

$$\mathbf{f}_{EE} = \frac{\partial \mathbf{P}}{\partial t} \times \mu_0 \mathbf{H} + \rho \mathbf{E} - \mu_0 \mathbf{H} \times \mathbf{J} - (\nabla \cdot \mathbf{P}) \mathbf{E} \quad (213)$$

$$\mathbf{f}_{ELE} = \frac{\partial \mathbf{P}}{\partial t} \times \mu_0 \mathbf{H} + \rho \mathbf{E} - \mu_0 \mathbf{H} \times \mathbf{J} + (\mathbf{P} \cdot \nabla) \mathbf{E} \quad (214)$$

Notice that (212) and (213) are identical, not so for the magnetic material case. One would anticipate the correct form should be easy to establish from an experiment. Note also that (212) uses $\nabla \cdot \mathbf{P}$ and the others $\mathbf{P} \cdot \nabla$, an issue that experiments should be able to distinguish. A related issue is to what degree (87) can be used, where the additional contributions to the stress tensor implicit in the Einstein-Laub formulation are ignored. For homogeneous media single plane waves normally incident on interfaces, (212) and (214) are identical, because $(\mathbf{P} \cdot \nabla) \mathbf{E} = 0$ and $(\nabla \cdot \mathbf{P}) \mathbf{E} = 0$. For monochromatic (time harmonic) waves, the magnitude of the first terms in (212) - (214) are identical.

The experimental evidence is as follows.

1. We used the Einstein-Laub form in (94), based on the Abraham momentum, to describe the Jones and Leslie experiments [22] - see [54] - see Section 11.1. However, the Lorentz form in (41) can equally well be used because the model relied only on the $\mu_0 \mathbf{H} \times \mathbf{J}$ term. Now we have derived a candidate expression based on the Minkowski momentum, we find that (117) can also be used with equal validity.
2. The change in focus of a Gaussian beam incident on water in a set of experiments from Ashkin is a very important experiment in evaluating candidate force expressions [71]. Section 11.2 describes our work and we find that the Einstein-Laub formulation describes this result. This result indicates that (214) is correct and that (212) and (213) are incorrect.
3. Atoms have been measured to have a recoil momentum of $n\hbar k_0$ [25], important in atom interferometry with optical gratings and consistent with the deBroglie momentum. Based on this work, one may conclude that the Minkowski momentum form might therefore appropriate. In

Section 11.3, we showed that the Einstein-Laub form with the Abraham momentum describes the pressure on a thin dielectric slab as being proportional to the background refractive index, supporting the result that the momentum imparted is also proportional to the background index. We should note that the background permeability was assumed unity, so the requirements for a negative index are not met. We have previously shown that the Einstein-Laub form leads to the conclusion that the sign of the force does not change with change in refractive index sign [16, 57]. This suggests that (214) can be used to explain the atom recoil [25].

We conclude that the optical experimental evidence to date supports use of the Einstein-Laub force density in (94) to describe forces on stationary, locally homogenized media. An open issue is whether the dispersion ($\partial\mathbf{P}/\partial t$) is correctly treated.

Another major open issue has been that the Einstein-Laub force density appeared not to have the $\mathbf{J} \times \mathbf{B}$ form consistent with magnetostatics [6], whereas experiments where the magnetization was shown to deflect an electron beam [42, 43]. In Section 4.3 of this report, we show that the Einstein-Laub force density can be couched in the form consistent with experimental evidence related to the Lorentz force for the first time. While there appears to be a need for additional experimental evidence related to forces with homogenized magnetic materials, at this stage the Einstein-Laub force density is the most credible theory to explain experiments, and (94) is

$$\mathbf{f}_{EL} = \frac{\partial\mathbf{P}}{\partial t} \times \mu_0\mathbf{H} - \frac{\partial\mu_0\mathbf{M}}{\partial t} \times \epsilon_0\mathbf{E} + \rho\mathbf{E} - \mu_0\mathbf{H} \times \mathbf{J} + (\mathbf{P} \cdot \nabla)\mathbf{E} + \mu_0(\mathbf{M} \cdot \nabla)\mathbf{H}.$$

References

- [1] A. Einstein and J. Laub, “Über die im elektromagnetischen Felde auf ruhende Körper ausgeübten ponderomotorischen Kräfte,” *Ann. Phys.* **331**, 541–550 (1908). English commentary on this paper and a reprint of the original paper appears in *The Collected Papers of Albert Einstein* (Princeton University Press, Princeton, NJ, 1989), Vol. 2.
- [2] W. Shockley, “Hidden linear momentum related to the $\vec{\alpha} \cdot \vec{e}$ term for a Dirac-electron wave packet in an electric field,” *Phys. Rev. Lett.* **20**, 343–346 (1968).
- [3] S. F. Nrelykke and H. Flyvbjerg, “Power spectrum analysis with least-squares fitting: Amplitude bias and its elimination, with application to optical tweezers and atomic force microscope cantilevers,” *Review of Scientific Instruments* **81**, 075103 (2010).
- [4] A. Mashghi, P. J. Vach, and S. J. Tans, “Noise reduction by signal combination in fourier space applied to drift correction in optical tweezers,” *Review of Scientific Instruments* **82**, 115103 (2011).
- [5] H. A. Lorentz, *The Theory of Electrons* (Dover, 1952), 2nd ed. These are notes from lectures given at Columbia University in the spring of 1906, as collected by H. A. Lorentz in 1909 and then in revised form in 1915.
- [6] P. Penfield and H. A. Haus, *Electrodynamics of Moving Media* (MIT Press, Cambridge, MA, 1967).

- [7] J. P. Gordon, “Radiation forces and momenta in dielectric media,” *Phys. Rev. A* **8**, 14–21 (1973).
- [8] I. Brevik, “Experiments in phenomenological electrodynamics and the electromagnetic energy-momentum tensor,” *Phys. Rep.* **52**, 133–201 (1979).
- [9] M. Mansuripur, “Radiation pressure and the linear momentum of the electromagnetic field,” *Opt. Express* **12**, 5375–5401 (2004).
- [10] R. Loudon, S. M. Barnett, and C. Baxter, “Radiation pressure and momentum in dielectrics: the photon drag effect,” *Phys. Rev. A* **71**, 063802 (2005).
- [11] R. N. C. Pfeifer, T. A. Nieminen, N. R. Heckenberg, and H. Rubinsztein-Dunlop, “Momentum of an electromagnetic wave in dielectric media,” *Rev. Mod. Phys.* **79**, 1197–1216 (2007).
- [12] B. A. Kemp, J. A. Kong, and T. M. Grzegorzczuk, “Reversal of wave momentum in isotropic left-handed media,” *Phys. Rev. A* **75**, 053810 (2007).
- [13] M. Mansuripur, “Resolution of the Abraham-Minkowski controversy,” *Opt. Comm.* **283**, 1997–2005 (2010).
- [14] C. Baxter and R. Loudon, “Radiation pressure and photon momentum in dielectrics,” *J. Mod. Opt.* **57**, 830–842 (2010).
- [15] S. M. Barnett, “Resolution of the Abraham-Minkowski dilemma,” *Phys. Rev. Lett.* **104**, 070401 (2010).
- [16] K. J. Webb and Shivanand, “Negative electromagnetic plane-wave force in gain media,” *Phys. Rev. E* **84**, 057602 (2011).
- [17] K. J. Webb and Shivanand, “Electromagnetic plane-wave forces on homogeneous material,” *J. Opt. Soc. Am. B* **29**, 1904–1910 (2012).
- [18] K. J. Chau and H. J. Lezec, “Revisiting the Balazs thought experiment in the case of a left-handed material: electromagnetic-pulse-induced displacement of a dispersive, dissipative negative-index slab,” *Opt. Express* **20**, 10138–10162 (2012).
- [19] M. Mansuripur, “Trouble with the lorentz law of force: incompatibility with special relativity and momentum conservation,” *Phys. Rev. Lett.* **108**, 193901 (2012).
- [20] B. Kemp, “Resolution of the abraham-minkowski debate: Implications for the electromagnetic wave theory of light in matter,” *Journal of Applied Physics* **109**, 111101 (2011).
- [21] E. F. Nichols and G. F. Hull, “The pressure due to radiation,” *Proc. Am. Acad. Arts Sci.* **38**, 559–599 (1903).
- [22] R. V. Jones and B. Leslie, “The measurement of optical radiation pressure in dispersive media,” *Proc. Royal Soc. A* **360**, 347–363 (1978).
- [23] A. Ashkin, J. M. Dziedzic, J. E. Bjorkholm, and S. Chu, “Observation of a single-beam gradient force optical trap for dielectric particles,” *Opt. Lett.* **11**, 288–290 (1986).
- [24] D. G. Grier, “A revolution in optical manipulation,” *Nature* **424**, 810–816 (2003).

- [25] G. K. Campbell, A. E. Leanhardt, J. Mun, M. Boyd, E. W. Streed, W. Ketterle, and D. E. Pritchard, “Photon recoil momentum in dispersive media,” *Phys. Rev. Lett.* **94**, 170403 (2005).
- [26] V. G. Veselago, “Energy, linear momentum, and mass transfer by an electromagnetic wave in a negative-refraction medium,” *Physics-Uspekhi* **52**, 649–654 (2009).
- [27] V. Yannopoulos and P. G. Galiatsatos, “Electromagnetic forces in negative-refractive-index metamaterials: a first-principles study,” *Phys. Rev. A* **77**, 043819 (2008).
- [28] R. W. Ziolkowski, “Superluminal transmission of information through an electromagnetic metamaterial,” *Phys. Rev. E* **63**, 046604 (2001).
- [29] R. Loudon and S. M. Barnett, “Theory of the radiation pressure on dielectric slabs, prisms and single surfaces,” *Opt. Express* **14**, 11855–11869 (2006).
- [30] M. Mansuripur and A. R. Zakharian, “Energy, momentum, and force in classical electrodynamics: application to negative-index media,” *Opt. Commun.* **283**, 4594–4600 (2010).
- [31] G. Bressi, G. Carugno, R. Onofrio, and G. Ruoso, “Casimir force between parallel metallic surfaces,” *Phys. Rev. Lett.* **88**, 041804 (2002).
- [32] M. L. Povinelli, M. Lončar, M. Ibanescu, E. J. Smythe, S. G. Johnson, F. Capasso, and J. D. Joannopoulos, “Evanescent-wave bonding between optical waveguides,” *Opt. Lett.* **30**, 3042–3044 (2005).
- [33] M. Scalora, G. D’Aguanno, N. Mattiucci, M. J. Bloemer, M. Centini, C. Sibilia, and J. W. Haus, “Radiation pressure of light pulses and conservation of linear momentum in dispersive media,” *Phys. Rev. E* **73**, 056604 (2006).
- [34] L. J. Chu, H. A. Haus, and P. Penfield, “The force density in polarizable and magnetizable fluids,” *Proc. IEEE* **54**, 920–935 (1966).
- [35] A. Mizrahi and Y. Fainman, “Negative radiation pressure on gain medium structures,” *Opt. Lett.* **35**, 3405–3407 (2010).
- [36] J. D. Jackson, *Classical Electrodynamics* (Wiley, New York, NY, 1999), 3rd ed.
- [37] A. Serdyukov, I. Semchenko, S. Tretyakov, and A. Sihvola, *Electromagnetics of Bi-Anisotropic Materials: Theory and Applications*, vol. 11 of *Electrocomponent Science Monographs* (Gordon and Breach Science Publishers, Amsterdam, 2001).
- [38] E. C. Titchmarsh, *The Theory of Functions* (Oxford University Press, 1932).
- [39] W. K. H. Panofsky and M. Phillips, *Classical Electricity and Magnetism* (Addison-Wesley, 1962).
- [40] H. W. Fuller and M. E. Hale, “Determination of magnetization distribution in thin films using electron microscopy,” *Journal of Applied Physics* **31** (1960).
- [41] F. Rasetti, “Deflection of mesons in magnetized iron,” *Phys. Rev.* **66**, 1–5 (1944).
- [42] M. S. Cohen, “Lorentz microscopy of small ferromagnetic particles,” *Journal of Applied Physics* **36** (1965).
- [43] M. Cohen, “Magnetic measurements with lorentz microscopy,” *Magnetics, IEEE Transactions on* **1**, 156–167 (1965).

- [44] M. Mansuripur, “Electromagnetic-force distribution inside matter,” *Phys. Rev. A* **88**, 023826 (2013).
- [45] M. Mansuripur, “The force law of classical electrodynamics: Lorentz versus Einstein and Laub,” in “Proc. of SPIE Vol. 8810, 88100K: Optical Trapping and Optical Micromanipulation X,” (2013).
- [46] M. Abraham, *Rend. Circ. Mat. Palermo* **28**, 1 (1909).
- [47] M. Abraham, *Rend. Circ. Mat. Palermo* **30**, 33 (1910).
- [48] H. Minkowski, “Die grundgleichungen für die elektromagnetischen vorgänge in bewegten körpern,” *Nachr. Ges. Wiss. Göttingen Math.-Phys. Kl.* pp. 53–111 (1908).
- [49] H. Minkowski, *Math. Ann.* **68**, 472 (1910).
- [50] J. J. Sakurai, *Modern Quantum Mechanics* (Benjamin/Cummings, Menlo Park, California, 1985).
- [51] J. C. Garrison and R. Y. Chiao, “Canonical and kinetic forms of the electromagnetic momentum in an *ad hoc* quantization scheme for a dispersive dielectric,” *Phys. Rev. A* **70**, 053826 (2004).
- [52] S. M. Barnett, “Resolution of the Abraham-Minkowski dilemma,” *Phys. Rev. Lett.* **104**, 070401 (2010).
- [53] P. W. Milonni and R. W. Boyd, “Recoil and photon momentum in a dielectric,” *Laser Physics* **15**, 1432–1438 (2005).
- [54] K. J. Webb, “Dependence of the radiation pressure on the background refractive index,” *Phys. Rev. Lett.* **111**, 043602 (2013).
- [55] M. Mansuripur, “Radiation pressure and the linear momentum of the electromagnetic field,” *Opt. Express* **12**, 5375–5401 (2004).
- [56] M. Mansuripur and A. R. Zakharian, “Whence the Minkowski momentum?” *Opt. Comm.* **283**, 3557–3563 (2010).
- [57] Shivanand and K. J. Webb, “Electromagnetic plane-wave force on a slab having various constitutive parameters and embedded in a background material,” *J. Opt. Soc. Am. B* **29**, 3330–3334 (2012).
- [58] C. Baxter and R. Loudon, “Radiation pressure and the photon momentum in dielectrics,” *J. Mod. Opt.* **57**, 830–842 (2010).
- [59] M. Mansuripur, “Trouble with the Lorentz law of force: incompatibility with special relativity and momentum conservation,” *Phys. Rev. Lett.* **108**, 193901 (2012).
- [60] K. J. Webb and Shivanand, “Negative electromagnetic plane-wave force in gain media,” *Phys. Rev. E* **84**, 57602 (2011).
- [61] K. J. Webb and Shivanand, “Electromagnetic field energy in dispersive materials,” *J. Opt. Soc. Am. B* **27**, 1215–1220 (2010).

- [62] L. Allen, M. W. Beijersbergen, R. J. C. Spreeuw, and J. P. Woerdman, “Orbital angular momentum of light and the transformation of laguerre-gaussian laser modes,” *Phys. Rev. A* **45**, 8185–8189 (1992).
- [63] N. B. Simpson, K. Dholakia, L. Allen, and M. J. Padgett, “Mechanical equivalence of spin and orbital angular momentum of light:an optical spanner,” *Opt. Lett.* **22**, 52–54 (1997).
- [64] M. E. J. Friese, T. A. Nieminen, N. R. Heckenberg, and H. Rubinsztein-Dunlop, “Optical torque controlled by elliptical polarization,” *Opt. Lett.* **23**, 1–3 (1998).
- [65] M. E. J. Friese, J. Enger, H. Rubinsztein-Dunlop, and N. R. Heckenberg, “Optical angular-momentum transfer to trapped absorbing particles,” *Phys. Rev. A* **54**, 1593–1596 (1996).
- [66] S. Chang and S. S. Lee, “Optical torque exerted on a homogeneous sphere levitated in the circularly polarized fundamental-mode laser beam,” *J. Opt. Soc. Am. B* **2**, 1853–1860 (1985).
- [67] I. Liberal, I. Ederra, R. Gonzalo, and R. W. Ziolkowski, “Electromagnetic force density in electrically and magnetically polarizable media,” *Phys. Rev. A* **88**, 053808 (2013).
- [68] R. A. Beth, “Mechanical detection and measurement of the angular momentum of light,” *Phys. Rev.* **50**, 115–125 (1936).
- [69] K. J. Webb, “Dependence of the radiation pressure on the background refractive index,” *Phys. Rev. Lett.* **111**, 043602 (2013).
- [70] A. Ludwig and K. J. Webb, “Accuracy of effective medium parameter extraction procedures for optical metamaterials,” *Phys. Rev. B* **81**, 113103 (2010).
- [71] A. Ashkin and J. M. Dziedzic, “Radiation pressure on a free liquid surface,” *Phys. Rev. Lett.* **30**, 139–142 (1973).
- [72] R. Loudon, “Theory of the forces exerted by laguerre-gaussian light beams on dielectrics,” *Phys. Rev. A* **68**, 013806 (2003).
- [73] R. Loudon, “Radiation pressure and momentum in dielectrics,” *Fortschritte der Physik* **52**, 1134–1140 (2004).
- [74] B. E. Saleh, M. C. Teich, and B. E. Saleh, *Fundamentals of Photonics*, vol. 22 (Wiley New York, 1991).
- [75] W. Erikson and S. Singh, “Polarization properties of Maxwell-Gaussian laser beams,” *Phys. Rev. E* **49**, 5778 (1994).
- [76] “COMSOL Multiphysics,” <http://www.comsol.com/products/multiphysics/>.
- [77] P. B. Johnson and R. W. Christy, “Optical constants of the noble metals,” *Phys. Rev. B* **6**, 4370–4379 (1972).
- [78] K. J. Webb and J. Li, “Waveguide cavity surface-enhanced raman scattering,” *Phys. Rev. B* **73**, 073404 (2006).